Primary photodissociation pathways of epichlorohydrin and analysis of the C–C bond fission channels from an O(^{3}P)+allyl radical intermediate

Benjamin L. FitzPatrick,[1] Bridget W. Alligood,[1] Laurie J. Butler,[1,a)] Shih-Huang Lee,[2] and Jim Jr-Min Lin[3]
[1]*Department of Chemistry and The James Franck Institute, University of Chicago, Chicago, Illinois 60637, USA*
[2]*National Synchrotron Radiation Research Center, Hsinchu 30076, Taiwan*
[3]*Institute of Atomic and Molecular Sciences, Academia Sinica, Taipei, Taiwan 10617, Republic of China*

(Received 18 February 2010; accepted 14 July 2010; published online 7 September 2010)

This study initially characterizes the primary photodissociation processes of epichlorohydrin, c-(H_2COCH)CH_2Cl. The three dominant photoproduct channels analyzed are c-(H_2COCH)CH_2 +Cl, c-(H_2COCH)+CH_2Cl, and C_3H_4O+HCl. In the second channel, the c-(H_2COCH) photofission product is a higher energy intermediate on C_2H_3O global potential energy surface and has a small isomerization barrier to vinoxy. The resulting highly vibrationally excited vinoxy radicals likely dissociate to give the observed signal at the mass corresponding to ketene, H_2CCO. The final primary photodissociation pathway HCl+C_3H_4O evidences a recoil kinetic energy distribution similar to that of four-center HCl elimination in chlorinated alkenes, so is assigned to production of c-(H_2COC)=CH_2; the epoxide product is formed with enough vibrational energy to isomerize to acrolein and dissociate. The paper then analyzes the dynamics of the C_3H_5O radical produced from C–Cl bond photofission. When the epoxide radical photoproduct undergoes facile ring opening, it is the radical intermediate formed in the O(^{3}P)+allyl bimolecular reaction when the O atom adds to an end C atom. We focus on the HCO+C_2H_4 and H_2CO+C_2H_3 product channels from this radical intermediate in this report. Analysis of the velocity distribution of the momentum-matched signals from the HCO+C_2H_4 products at m/e=29 and 28 shows that the dissociation of the radical intermediate imparts a high relative kinetic energy, peaking near 20 kcal/mol, between the products. Similarly, the energy imparted to relative kinetic energy in the H_2CO+C_2H_3 product channel of the O(^{3}P)+allyl radical intermediate also peaks at high-recoil kinetic energies, near 18 kcal/mol. The strongly forward-backward peaked angular distributions and the high kinetic energy release result from tangential recoil during the dissociation of highly rotationally excited nascent radicals formed photolytically in this experiment. The data also reveal substantial branching to an HCCH+H_3CO product channel. We present a detailed statistical prediction for the dissociation of the radical intermediate on the C_3H_5O potential energy surface calculated with coupled cluster theory, accounting for the rotational and vibrational energy imparted to the radical intermediate and the resulting competition between the H+acrolein, HCO+C_2H_4, and H_2CO+C_2H_3 product channels. We compare the results of the theoretical prediction with our measured branching ratios. We also report photoionization efficiency (PIE) curves extending from 9.25 to 12.75 eV for the signal from the HCO+C_2H_4 and H_2CO+C_2H_3 product channels. Using the C_2H_4 bandwidth-averaged absolute photoionization cross section at 11.27 eV and our measured relative photoion signals of C_2H_4 and HCO yields a value of 11.6+1/−3 Mb for the photoionization cross section of HCO at 11.27 eV. This determination puts the PIE curve of HCO measured here on an absolute scale, allowing us to report the absolute photoionization efficiency of HCO over the entire range of photoionization energies. © *2010 American Institute of Physics*. [doi:10.1063/1.3475001]

I. INTRODUCTION

The O(^{3}P)+allyl bimolecular reaction results in several competing product channels. Previous studies have sought to probe the product branching and dynamics of this reaction.[1–11] The complexity of the competition between bond fission and isomerization pathways is surprising for such a small system, composed of only four heavy atoms and five hydrogen atoms. Most of the prior studies[1,5–10] correctly identified the H+acrolein product channel as a major contributor to the overall product branching. However, just a few[7–10] examined those product channels resulting in C–C bond fission.

Much of the complication in reactions involving O(^{3}P) with hydrocarbons arises from the competition between direct abstraction and addition/elimination reactions, where the vibrationally excited radical intermediate formed in the addition mechanism may result in several possible product channels. Early bulk kinetics experiments by Slagle *et al.*[1]

a)Author to whom correspondence should be addressed. Electronic mail: l-butler@uchicago.edu.

measured the overall rate of the reaction from 300 to 600 K and detected the H+acrolein product channel using photoionization mass spectrometry. They correctly anticipated that C–C bond fission to form $H_2CO+C_2H_3$ might compete with C–H bond fission, but were unable to detect signal at H_2CO or vinyl attributable to a primary channel so put an upper limit on it of <20% of the H+acrolein channel. Choi and co-workers[2,3] detected H atoms from this reaction and, interestingly, nascent OH radicals having two different rotational distributions. They assign the predominant pathway forming OH to direct abstraction, resulting in rotationally cooler OH, and a small, rotationally hot portion of the OH to addition/elimination pathways. Choi and co-workers calculated key portions of the O+allyl potential energy surface beginning with addition of the O atom to the central and terminal C atoms, respectively. Using 17 eV electron bombardment ionization, later crossed molecular beam studies by Casavecchia and co-workers[7,8] at a high collision energy of 73.0 kJ mol^{-1} sought to detect the product channels predicted in Choi's theoretical work. They characterized the H+acrolein product channel and detected evidence for two C–C bond fission channels. Their signals at m/e=27 and 29 showed a large peak near the center-of-mass scattering angle due to dissociative ionization of acrolein and a smaller forward scattered component. The authors note[8] that the forward scattered signal at m/e=29 might be due to either dissociative ionization of formaldehyde from the $H_2CO+C_2H_3$ product channel or to HCO from the $HCO+C_2H_4$ product channel. Although they suggest it is primarily due to the latter, we note that dissociation of the HCO radical to H+CO requires only 15 kcal/mol, and the O+allyl reaction producing $HCO+C_2H_4$ is exoergic by over 75 kcal/mol, so it is unlikely that stable HCO product contributes significantly to that signal. Later bulk kinetics work in 2009 by Hoyermann *et al.*[10] used laser flash photolysis to generate the O and allyl reactants and measured the rate constant for the reaction from 300 to 623 K. They also measured the branching to the stable end products of the reaction by quantitative FTIR spectroscopy at room-temperature to be 47% to H+acrolein, 41% to $H+CO+C_2H_4$, 7% to $H_2CO+C_2H_3$, and <5% to H_2CCCH_2+OH. Our first paper[9] on this system, published in 2008, was motivated by a need to gain insight into these dynamics. Choi's theoretical work showed that the highly exothermic O+allyl reaction may proceed through several intermediate transition states en route to the final products. Indeed, the competition between the intermediate isomerization and dissociation pathways of the initially formed C_3H_5O radical adduct controls the subsequent product channel branching observed for the bimolecular reaction. Thus, we[9] initiated the reaction from the radical intermediate formed from addition of the O atom to the end C atom of allyl, but at lower internal energies than would be formed in the bimolecular collision. This allowed us to clearly distinguish between the contributing C–C fission product channels using tunable vacuum-ultraviolet (VUV) photoionization (the data also measured the branching to the H+acrolein product channel). The data showed that the most exothermic product channel $CO+C_2H_5$ does not contribute to the product branching, while $HCO+C_2H_4$ and $H_2CO+C_2H_3$ do. The work presented herein continues to focus on the radical intermediate formed in the entrance channel for the barrierless addition of an $O(^3P)$ atom to a terminal carbon, the OCH_2CHCH_2 radical intermediate, INT1, shown in Fig. 1.

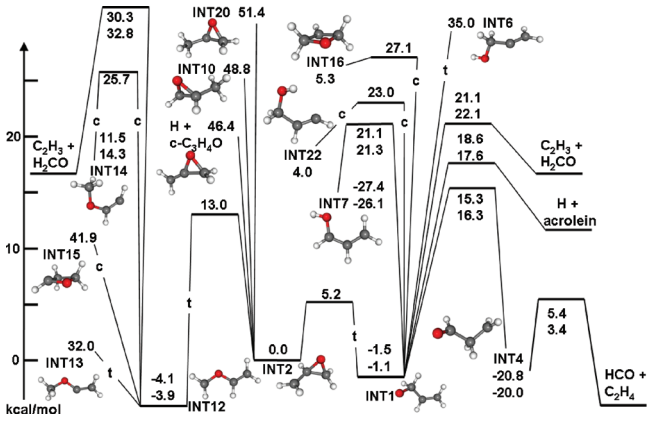

FIG. 1. Some minima and transition states on the PES of the $O(^3P)$+allyl reaction. The figure is centered on the INT2 intermediate, which is also taken as the zero of energy. Any intermediate or transition state having *cis* and *trans* conformers has both energies listed, with *cis* being the upper number and *trans* the lower. The transition states that only link one of the conformers have a letter designation. For example, INT2 is only linked to the *trans* conformer of INT12. The transition states lying higher than 31 kcal/mol are truncated to keep the PES as compact as possible, and the energy listed is the barrier height. The geometries and harmonic vibrational frequencies were computed using UCCSD/aug-cc-pVDZ, and single point energies were calculated using UCCSD(T)-F12B/cc-pVQZ-F12 with a complete-basis-set extrapolation for the perturbative triples (see text for complete details). The energies shown include a harmonic zero-point energy correction.

In order to discern the dynamics of the O+allyl reaction through its competing addition/elimination product channels, we thus do not begin with a bimolecular collision. Instead we photolytically produce a radical intermediate of the bimolecular reaction, so that it is formed with lower internal energies on the global potential energy surface. Using photodissociation of a halogenated precursor, our experiments produce c-$(H_2COCH)CH_2$ radicals (INT2 in Fig. 1) that undergo facile isomerization to the OCH_2CHCH_2 radical intermediate (INT1 in Fig. 1) of the O+allyl bimolecular reaction. Radical intermediates produced in this way have enough internal energy to access the dominant observed product channels of the bimolecular reaction, but far less energy than the 75 kcal/mol internal energy of this radical intermediate when produced in the bimolecular collision. This specificity in the radical intermediate and its internal energy distribution allows us to probe the competing pathways of the addition/elimination reaction at energies sensitive to the intermediate transition states calculated for the bimolecular reaction.

II. EXPERIMENT

The velocity distributions of the epichlorohydrin photofragments were measured using the rotating-source, crossed laser-molecular beam apparatus[12–16] on the 21A1 U9/Chemical Dynamics Beamline at the National Synchrotron Radiation Research Center (NSRRC) located in Hsinchu, Taiwan. A Lambda Physik LPX 220 ArF laser, operating at

193.3 nm, produced momentum-matched photofragment pairs, such as Cl atoms and C_3H_5O radicals, by photodissociation of epichlorohydrin, Fluka >98% purity. The laser operated at 80 Hz with a measured output ranging from 7 to 9 mJ per pulse. Given epichlorohydrin's small absorption cross section at 193 nm, on the order of 10^{-19} cm^2, and the above pulse energies, these experiments were well below saturation. The focused laser beam was a rectangle 8.5 mm tall × 2.5 mm wide, which intersected the ~3 mm diameter molecular beam. The molecular beam was generated by bubbling helium through room-temperature, liquid epichlorohydrin, and expanding this mixture through an Even–Lavie pulsed valve. The backing pressure of helium was 800 torr, and the pulsed valve had an orifice of 0.25 mm in diameter and was heated to 110 °C.

The molecular beam's speed distribution at the maximum of the pulse was determined using a chopper wheel nominally operating at 200 Hz. The peak in the number density distribution of molecular speeds was 1590 m/s with a full-width-at-half-maximum of 21.0%. The peak speed is similar to that in the 2006 experiments,[9] but the distribution is narrower, which indicates that the supersonic expansion in these experiments more effectively cooled the internal degrees of freedom. Aside from the above difference in the width of the speed distribution, the different expansion also led to a slightly different recoil kinetic energy distribution needed to fit the Cl atom time of flight spectra. This difference will be discussed further in Sec. IV D. Only a small number of recoiling photofragments, those having the proper velocity after photodissociation to enter the detector, travel the 10.05 cm neutral flight path where tunable vacuum-ultraviolet synchrotron radiation ionized them. Photoionization energies were tuned with the U9 undulator gap, and a 7 mm diameter circular aperture defined the VUV beam. In this work a 33 mm gap was used to obtain a nominal photoionization energy of 13.78 eV. A rare gas filter, consisting of approximately 10 torr of Ar or Kr, filtered out higher harmonics of the VUV. In addition to the rare gas filter, an MgF_2 window was inserted into the VUV beam when the photon energy was tuned below 9.75 eV. After traveling through the ionization region, the photofragments were mass selected using an Extrel 1.7 MHz quadrupole mass spectrometer and were counted by a Daly detector.[17] A multichannel scaler recorded the total time-of-flight (TOF) of the photofragments spent in traveling from the interaction region to the Daly detector. There was a time lag of 2.40 μs between triggering of the multichannel scaler and firing of the laser, for which all TOF spectra and associated fits are corrected. The flight times depicted in the figures herein are the sum of the neutral photofragment flight time (from a velocity determined by the vector sum of the center-of-mass velocity, the recoil velocity imparted during photodissociation, and, for bimolecular products, the recoil velocity imparted to product as the radical unimolecularly dissociates) and the ion flight time through the mass spectrometer. The latter is calculated using the apparatus' measured ion flight constant of 5.40 μs $amu^{-1/2}$. The recoil translational energy distribution from the C–Cl bond fission is determined by creating a forward convolution fit to the TOF spectra. Finally, the conservation of energy yields an internal energy distribution of the nascent C_3H_5O radicals.

III. COMPUTATIONAL METHOD

The electronic structure methods employed herein will be discussed briefly. The Gaussian-3 (G3//B3LYP) (Refs. 18 and 19) method, implemented in GAUSSIAN03,[20] was used for all ionization and appearance energies as it accurately calculates such ion energetics. G3//B3LYP was also used for some potential energy surface (PES) calculations in cases where very accurate barrier heights are not needed. Even though G3//B3LYP was not designed for calculating accurate barrier heights it performs reasonably well.

When higher accuracy stationary points on a PES were required, such as in the partial PES of $O(^3P)$+allyl shown in Fig. 1, open-shell coupled cluster was employed. All geometries and harmonic vibrational frequencies were calculated using spin unrestricted coupled cluster with singles and doubles (UCCSD) and the aug-cc-pVDZ basis sets in GAUSSIAN03. Each harmonic zero-point vibrational energy (ZPE) was scaled by 0.98 in accord with the work of Radom *et al.*[21] All geometries were also calculated using B3LYP/aug-cc-pVDZ, and this method was used when performing intrinsic reaction coordinate calculations to make sure all transition states connect the correct intermediates. Single point energies were calculated using the coupled-cluster programs within MOLPRO 2008.1 (Ref. 22). The complete basis set limit of the restricted, open-shell Hartree–Fock energy and the UCCSD energy were calculated using their implementation of explicitly correlated UCCSD-F12B (Refs. 23 and 24) and the cc-pVQZ-F12 basis sets of Peterson *et al.*[25] The contribution of the perturbative triples was calculated using MOLPRO's[26] UCCSD(T)/aug-cc-pVNZ, where N=2 or 3, and extrapolated to the complete basis set limit via the method of Schwenke.[27] Readers interested in more of the calculation and PES details can find them in our theoretical investigation[11] of the $O(^3P)$+allyl/OH+allene potential energy surface.

IV. RESULTS ON THE PRIMARY PHOTODISSOCIATION CHANNELS

A. Energetics of some possible photodissociation channels of epichlorohydrin

While the focus of this study is the Cl + c-$(H_2COCH)CH_2$, INT2 in Fig. 1, channel given in Eq. (1), it is helpful to consider the other primary photodissociation channels listed below in Eqs. (2) and (3b). The more uncommon fragments below are displayed in Fig. 2 along with their molecular formulas and names,

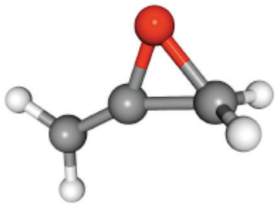

c-$(H_2COC)CH_2$
2-methyleneoxirane

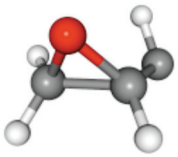

c-$(H_2COCH)CH$
2-methineoxirane

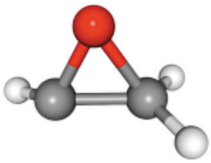

c-H_2COCH
oxiranyl radical

FIG. 2. Structures, molecular formulas, and names of three possible primary photodissociation products.

$$\text{c-}(H_2COCH)CH_2Cl \rightarrow \text{c-}(H_2COCH)CH_2 + Cl(^2P_{3/2,1/2}) \quad (1)$$

$$\Delta H_{rxn} = 80.1 \text{ kcal/mol},$$

$$\rightarrow \text{c-}CH_2OCH + CH_2Cl \quad \Delta H_{rxn} = 92.3 \text{ kcal/mol}, \quad (2)$$

$$\rightarrow CH_2 = CHCH = O + HCl \quad \Delta H_{rxn} = -10.7 \text{ kcal/mol}, \quad (3a)$$

$$\rightarrow \text{c-}(H_2COC) = CH_2 + HCl \quad \Delta H_{rxn} = 18.0 \text{ kcal/mol}, \quad (3b)$$

$$\rightarrow \text{c-}(H_2COCH)CH + HCl \quad \Delta H_{rxn} = 83.5 \text{ kcal/mol}. \quad (3c)$$

The enthalpy differences were calculated using the G3//B3LYP method at 0 K. The calculated[9] bond dissociation energy of the carbon-chlorine bond in epichlorohydrin is 80.1 kcal/mol. Two of the HCl elimination channels have much lower endoergicities than the C–Cl [Eq. (1)] and C–C [Eq. (2)] simple bond fission channels. The five-center elimination channel to form HCl+acrolein, the most stable C_3H_4O conformer, is exothermic. A four-center elimination mechanism, Eq. (3b), involving the center carbon and its lone hydrogen atom, gives 2-methyleneoxirane; this pathway also has a much lower reaction enthalpy in comparison with the other photodissociation channels. The above two HCl-loss pathways would partition 60–90 kcal/mol more energy into the nascent photofragments than would be possible with the other channels, while the three-center HCl elimination, Eq. (3c), is highly endothermic as it produces a biradical.

The above enthalpy differences, in combination with the total recoil kinetic energy distributions derived from our experiments, are crucial in determining the amount of internal energy apportioned to particular nascent photofragment pairs. The C–Cl bond fission events are considered first because the chlorine atoms may be formed in only two spin-orbit states, which simplifies the partitioning of internal energy between the Cl atoms and their C_3H_5O cofragments. Equation (4) details the energy balance in C–Cl bond fission events,

$$E_{int}(C_3H_5O) + E_T = E_{int}(\text{precursor}) + h\nu - \Delta H_{rxn} - E_{so}. \quad (4)$$

Of the two terms on the left, the recoil kinetic energy E_T is derived by fitting the measured velocity distribution of the Cl cofragment and imposing conservation of momentum, thereby leaving $E_{int}(C_3H_5O)$ as the only unknown. As for the terms on the right-hand side of Eq. (4), we assume that the supersonic expansion effectively cools the rotational motions, but leaves the vibrational energy thermalized at the nozzle temperature of 383 K. Using the harmonic vibrational frequencies calculated at the B3LYP/aug-cc-pVDZ level and scaled by a factor of 0.97,[21] these assumptions give $E_{int}(\text{precursor}) = 2.7$ kcal/mol. There are three possible conformers of the precursor molecule with different orientations of the chloromethyl group with respect to the cyclic ring. G3//B3LYP calculations predict that the relative stability of these three conformers differs by 0.6–1.2 kcal/mol. Thus, the conformers are indistinguishable given the experimental uncertainty in this study and the accuracy of the theoretical methods employed here. The photon energy $h\nu$ is 147.8 kcal/mol for 193.3 nm light. Equation (1) provides the reaction enthalpy of 80.1 kcal/mol [the energy difference between the most stable conformer of epichlorohydrin and INT2 $+Cl(^2P_{3/2})$]. Lastly, E_{so} is selected to be 0 or 2.5 kcal/mol, which correspond to the ground ($^2P_{3/2}$) and excited ($^2P_{1/2}$) spin-orbit state of the Cl atom. Application of Eq. (4) shows that, for the C–Cl bond fission channel, the nascent radical's internal energy is 70 kcal/mol minus the measured recoil kinetic energy E_T.

In the other primary photodissociation channels the internal energy is partitioned between two molecular photoproducts, so applying conservation of energy and linear momentum allows us to determine from the measured recoil kinetic energy only the sum of the internal energy partitioned to the two products, $E_{int}(\text{photofragments})$ [Eq. (5)]. First, the spin-orbit energy term must be removed because it should be negligible for any of the open-shell molecular species. E_{int} now sums the electronic, vibrational, and rotational energy of both photofragments together,

$$E_{int}(\text{photofragments}) + E_T = E_{int}(\text{precursor}) + h\nu - \Delta H_{rxn}. \quad (5)$$

The CH_2Cl pathway is the most endothermic, leaving 58 kcal/mol to be partitioned between E_T and E_{int}(photofragments). For the HCl-loss channel, the energy available for E_T and E_{int}(photofragments) varies from 161 kcal/mol for the first pathway, Eq. (3a), to 133 and 67 kcal/mol for the second and third pathways, Eqs. (3b) and (3c), respectively.

B. Determining the internal energy distribution of CH_2Cl+c-$HCOCH_2$

Our previous work[9] already discussed the internal energy distribution of the radicals produced in the C–Cl bond fission events, Eq. (1), so we now consider the internal energy partitioned to the photofragments formed from C–C bond fission [Eq. (2)] in this section and HCl elimination [Eq. (3)] in the next section. We return to the to the C–Cl bond fission channel, which forms the radical intermediate of the $O(^3P)$+allyl reaction, in Sec. IV D.

The top frame of Fig. 3 shows the measured time-of-flight spectrum of the CH_2Cl photofragments detected at m/e=49 using 11.27 eV photoionization. The C–C bond photofission reaction given in Eq. (2) produces CH_2Cl and c-$HCOCH_2$. We determine the distribution energies imparted to recoil kinetic energy $P(E_T)$ for this C–C bond fission channel by iteratively fitting the data in Fig. 3 (top). The resulting $P(E_T)$, shown in Fig. 4, extends from 0 kcal/mol to just over 20 kcal/mol. Equation (5) reveals that the momentum-matched cofragment c-$HCOCH_2$ could be formed with significant internal energy. The CH_2Cl and oxiranyl radicals share between 38 and 58 kcal/mol of internal energy across the kinetic energy distribution for C–C photofission. This leads us to consider the possibility that the oxiranyl radicals, momentum-matched to the CH_2Cl radicals, might have enough internal energy to dissociate.

Figure 5 shows the calculated transition states for the isomerization/dissociation channels of oxiranyl radicals. The calculations show that if the oxiranyl radicals are formed with as little as 13 kcal/mol of internal energy they isomerize to vinoxy. The resulting vinoxy radicals would have enough energy to be formed in the A state or in the ground electronic state. They are expected to dissociate to H+ketene via the A state,[28] and to CH_3+CO via isomerization to acetyl radicals on the ground state. (Oxiranyl radicals do not have enough energy to directly undergo H-atom loss to form oxirene+H; calculations by Tozer and Wilson[29] show that the H+oxirene dissociation products would lie 80 kcal/mol above the H+ketene product asymptote shown in Fig. 5.) The TOF spectrum in Fig. 3 (bottom frame), taken at m/e=42 (CH_2CO^+), is well fit by assuming that vibrationally excited oxiranyl radicals dissociate to H+ketene across the whole distribution of velocities of radicals produced in conjunction with CH_2Cl. The fit shown is calculated from the C–C bond fission recoil kinetic energy distribution, Fig. 4, derived from the CH_2Cl TOF spectrum. The oxiranyl radicals are momentum-matched to the CH_2Cl product, so when they isomerize and undergo H-atom loss the dissociation barely changes the velocity of the heavy ketene cofragment. Hence, the ketene product velocities are essentially momentum-matched to the CH_2Cl primary photoproduct, as shown by the fit in Fig. 3, bottom. The oxiranyl radicals may also dissociate to CH_3+CO, but we did not search for signal at m/e=28 with a photoionization energy sufficient to ionize CO.

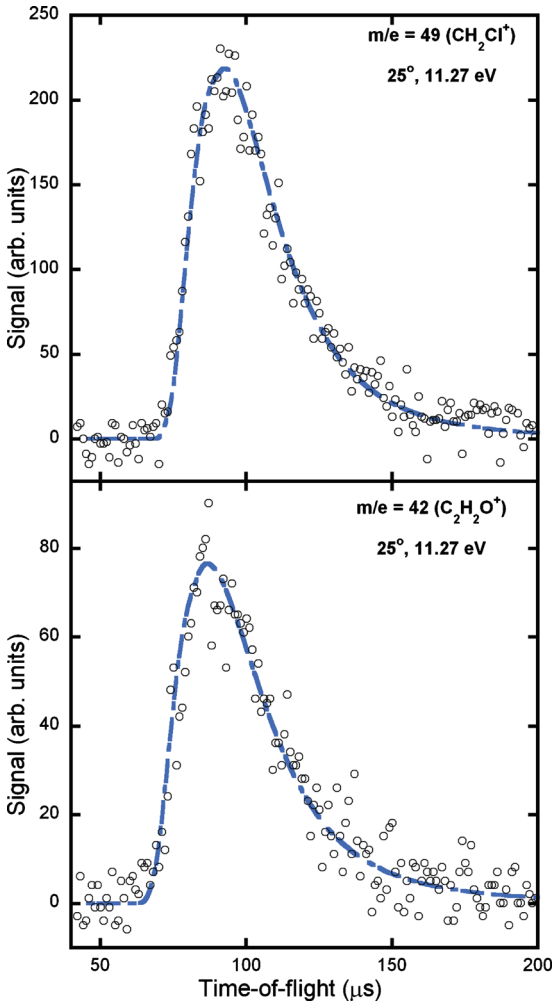

FIG. 3. TOF spectra of m/e=49 (CH_2Cl^+) and 42 (H_2CCO^+) at a source angle of 25°. These data were accumulated for 400 000 laser shots. A time-dependent background, accumulated for 150 000 laser shots, was subtracted from the m/e=49 data, while constant background subtraction sufficed for m/e=42. The open circles correspond to the data points and the dot-dashed line is the overall fit calculated from the $P(E_T)$ in Fig. 4.

C. Determining the internal energy distribution of the HCl+C_3H_4O photoproducts

While the C–C bond photofission channel CH_2Cl +c-$HCOCH_2$ in the prior section is straightforward, there are a multitude of possible HCl-loss routes. Figure 6 displays the fits to the m/e=36 data taken with a photoionization energies of 11.91 and 13.78 eV. The $P(E_T)$ in Fig. 7, derived from fitting the m/e=36 spectra in Fig. 6, is peaked below 10 kcal/mol and extends to nearly 50 kcal/mol. [The shape of the $P(E_T)$ below 3 kcal/mol is arbitrary because the fit to the data is insensitive to this region.] The general shape of the

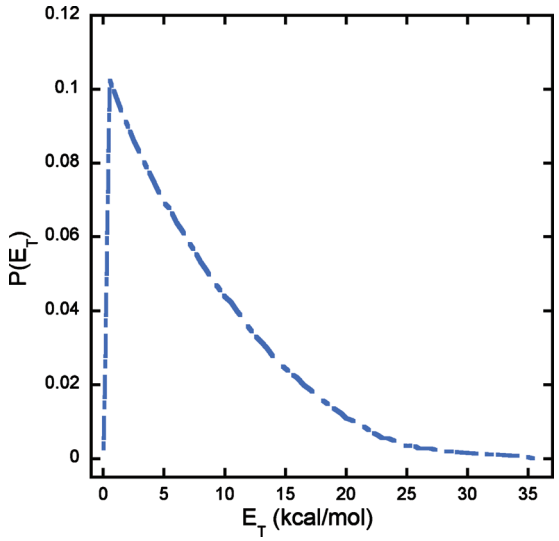

FIG. 4. Total recoil kinetic energy distribution for the primary photodissociation channel producing $CH_2Cl+c\text{-}CH_2OCH$. It was derived by forward-convolution fitting of the m/e=49 data in the top frame of Fig. 3. The $P(E_T)$ peaks near 0 kcal/mol and tails to zero just above 25 kcal/mol.

$P(E_T)$ is very similar to that found in four-center HCl loss from 2-chloropropene,[30] suggesting that HCl loss from epichlorohydrin occurs via a four-center mechanism. Based on the four-center elimination, nascent HCl and 2-methyleneoxirane fragments share between 83 and 133 kcal/mol of internal energy; of these, about 99% share more than 100 kcal/mol. The upper spectrum in Fig. 6 preferentially evidences HCl products having vibrational energies in excess of 20 kcal/mol because the peak photoionization energy of 11.91 eV is almost 1 eV below threshold.

The cofragment of the HCl product in a four-center HCl photoelimination channel is 2-methyleneoxirane. Vibrationally excited 2-methyleneoxirane may isomerize to acrolein over a barrier calculated (G3//B3LYP) to be 88.9 kcal/mol. Because 99% of the HCl+2-methyloxirane cofragments

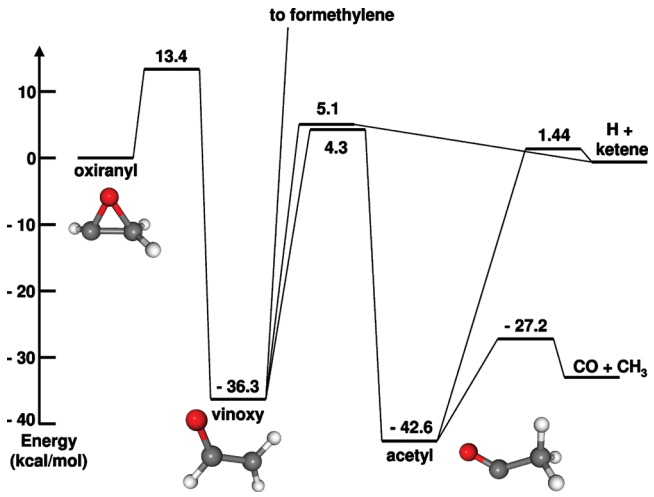

FIG. 5. Some critical points on the ground state C_2H_3O PES calculated using G3//B3LYP (including a harmonic ZPE correction). The oxiranyl radical is the C–C photofission cofragment formed in conjunction with CH_2Cl [Eq. (2)]. The figure shows if the oxiranyl radical is formed with only 13.4 kcal/mol of vibrational energy that it would isomerize and dissociate to either H+ketene or $CO+CH_3$.

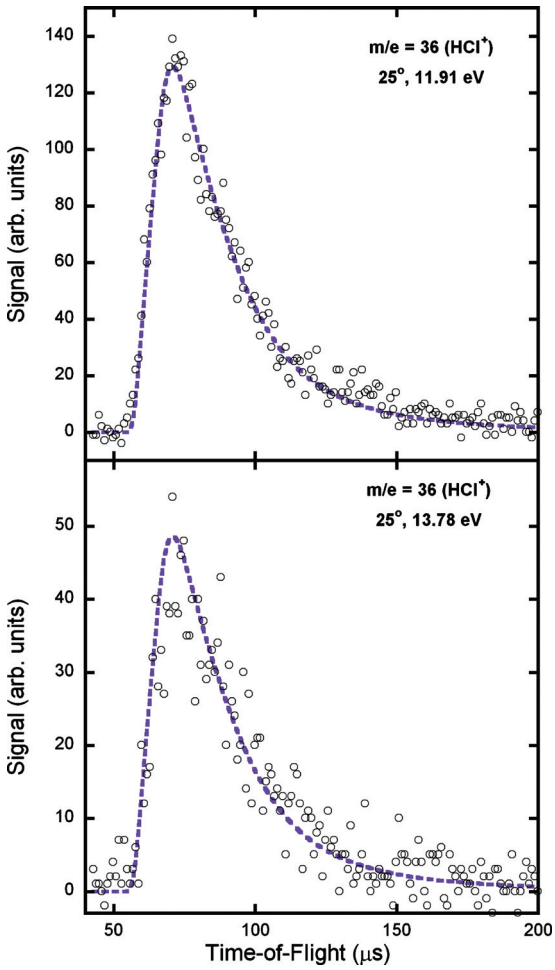

FIG. 6. TOF spectra of m/e=36, HCl^+ at a photoionization energy of 11.91 eV (upper frame) and 13.78 eV (lower frame). The 11.91 eV spectrum, taken in 2006, was accumulated for 200 000 laser shots. The spectrum at 13.78 eV, taken two years later, was accumulated for 100 000 laser shots. A constant background is subtracted from both spectra. The open circles represent the data points and the short-dashed line is the fit to the data calculated from the $P(E_T)$ shown in Fig. 7.

share over 100 kcal/mol of internal energy, we expect a substantial fraction of the HCl-elimination cofragments to isomerize to acrolein. This isomerization is exoergic by 28.7 kcal/mol, so any acrolein produced from the isomerization of 2-methyleneoxirane would dissociate. Indeed, apparently all of the mass 56 cofragments to the HCl photoproduct dissociate (none of the signal we detected at m/e=56 in Ref. 9 is momentum-matched to the HCl photoproducts). Some of the signal detected in the m/e=55 TOF spectrum presented in Sec. IV D evidences a velocity distribution that is well fit by assuming the signal results from the unimolecular dissociation of vibrationally excited acrolein (to $H+OC_3H_3$) produced in the HCl elimination channel.

D. Determining the internal energy distribution of the C_3H_5O radicals produced from C–Cl bond photofission

Figure 8 depicts the measured TOF spectrum at m/e =35, Cl^+. The data are similar to those measured two years earlier and published in Ref. 9. They evidence a high-recoil kinetic energy component, and a minor channel partitioning

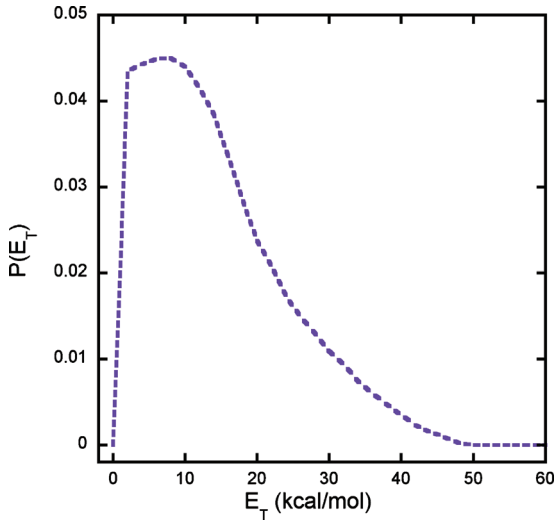

FIG. 7. Total recoil kinetic energy distribution derived from the forward convolution fit to the m/e=36 data in Fig. 6. The fit to the data is not sensitive to the shape of the $P(E_T)$ below a few kcal/mol, so that region of the $P(E_T)$ is arbitrary.

much lower energies to relative kinetic energy of the Cl $+C_3H_5O$ photoproducts. Our previous work[9] determined the $P(E_T)$ for the C–Cl bond photofission channel of epichlorohydrin at 193 nm using both 2+1 resonance enhanced multiphoton ionization of the Cl atoms in a velocity map imaging (VMI) experiment and single photon VUV ionization in an experiment identical to that reported here. In the VMI experiment, the Cl^+ signal showed the expected two-photon resonance enhancement, confirming that the signal was from the 2+1 ionization of neutral Cl atoms and not from dissociative ionization of a Cl-containing diatomic or polyatomic photoproduct. We weighted the recoil kinetic energy distributions of the $Cl(^2P_{3/2})+C_3H_5O$ and the $Cl(^2P_{1/2})+C_3H_5O$ channels in Ref. 9 by the measured Cl atom spin-orbit branching ratio; the resulting $P(E_T)$ was essentially identical to that determined from the m/e=35 TOF detected with

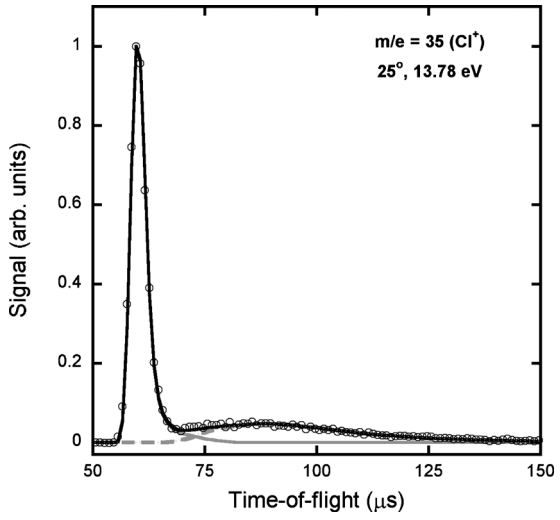

FIG. 8. TOF spectrum taken at m/e=35 (Cl^+) at a source angle of 25°. The data were accumulated for 150 000 laser shots and a constant background was subtracted. The open circles correspond to the data points and the fit is calculated from the C–Cl bond fission $P(E_T)$ shown in black line in Fig. 9.

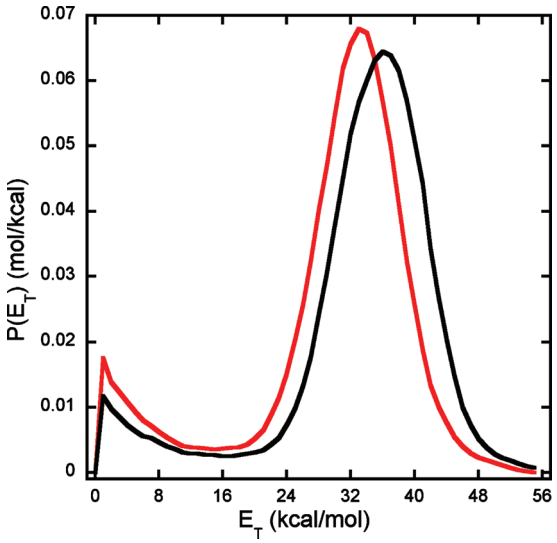

FIG. 9. Comparison of the C–Cl bond photofission $P(E_T)$ determined in our prior experiments (Ref. 9) with the one determined from a forward convolution fit to the new data in Fig. 8. Although they are similar, the higher kinetic energy peak in the newer $P(E_T)$ shown in black is shifted about 3 kcal/mol faster than the one published in Ref. 9, shown in red. As the VMI measurements accurately reproduced the $P(E_T)$ shown in red, we use that $P(E_T)$ for the analysis of the internal energy distribution of the momentum-matched C_3H_5O radicals in this work.

VUV photoionization at 13.8 eV. [The imaging experiments[9] showed that the $Cl(^2P_{1/2})$ and $Cl(^2P_{3/2})$ signals have similar angular distributions.] This correspondence of the two measurements, one of which relies on resonance-enhanced Cl atom ionization, demonstrates that the signal detected with VUV photoionization does not include any signal from dissociative ionization of the HCl or CH_2Cl photoproducts to Cl^+. Further note that the C–Cl bond energy in the CH_2Cl and HCl photoproducts is calculated (with G3//B3LYP) to be 92.4 and 102 kcal/mol, respectively, so neither of these photoproducts can dissociate to yield Cl atoms given the energy available to them. Thus, we assign the low-recoil kinetic energy portion of the $P(E_T)$, shown in Fig. 9, to C–Cl bond fission resulting in Cl atoms $+C_3H_5O$ radicals that form in an electronically excited state as the epoxide ring opens.[31] The dominant high-recoil kinetic energy portion of the $P(E_T)$ corresponds to Cl+c-$(H_2COCH)CH_2$ radicals in the ground electronic state; these radicals undergo facile ring opening to form the C_3H_5O radical adduct, INT1 in Fig. 1, which is a radical intermediate important in the O+allyl bimolecular reaction. The rest of this paper focuses on the dissociation channels of this radical intermediate.

Using Eq. (4) to determine the distribution of internal energies of the nascent c-$(H_2COCH)CH_2$ radicals formed in the dominant C–Cl bond fission channel, we must account for the radicals produced in conjunction with $Cl(^2P_{3/2})$ separately from those formed in conjunction with $Cl(^2P_{1/2})$. The VMI measurements presented in Ref. 9 allow us to do that; in this paper we use those results in conjunction with the $P(E_T)$ shown by the red line in Fig. 9, as they correspond closely. Even for the high-recoil kinetic energy portion of the C–Cl bond fission $P(E_T)$ extending from $E_T=20$ to 48 kcal/mol, the internal energy of the momentum-matched C_3H_5O radicals calculated from Eq. (4) ranges from 50 to

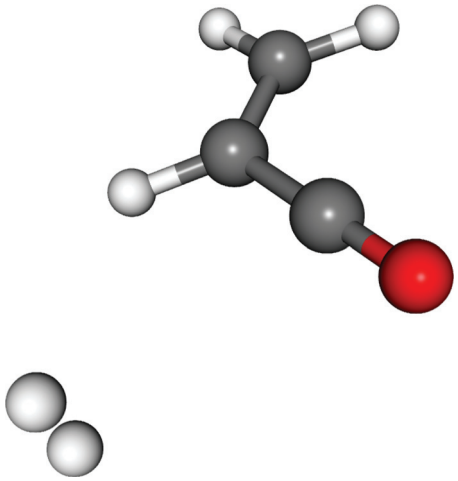

FIG. 10. Geometry of singlet $C_3H_5O^+$ starting from *cis*-INT1, optimized using B3LYP/aug-cc-pVDZ. (A nearly identical structure was found using an MP2 optimization.) Adiabatic and vertical ionization energies, calculated using G3//B3LYP, are 6.8 and 10.4 eV, respectively. The triplet cation has a structure similar to INT1.

23 kcal/mol. All of the radicals are formed with an internal energy above one or more of the barriers (see Fig. 1) that lead to products on the C_3H_5O potential energy surface. Indeed, we did not detect any signal from stable radicals at m/e=57. However, our prior analysis[9] of the partitioning of the total internal energy in the nascent radicals between vibration and rotation, refined in Sec. V A, indicated that the radicals were formed with substantial energy partitioned to rotational energy. Thus, we considered the possibility that there might be some stable radicals produced. To assess the possibility that any stable radicals, produced in the highest recoil kinetic energy C–Cl bond photofission events, might undergo dissociative photoionization we performed a geometry optimization of the singlet C_3H_5O cation at the B3LYP/aug-cc-pVDZ level. The equilibrium geometry, shown in Fig. 10, reveals a structure where a core C_3H_3O cation is weakly bound to an H_2 moiety, so we searched for signal from stable C_3H_5O radicals at the m/e=55 daughter ion. Although our experiments detected a substantial amount of m/e=55 signal, it did not show a sharp peak in the TOF spectrum between 75 and 80 μs. This is the expected range of arrival times, invoking conservation of momentum with the Cl atoms detected in Fig. 8 above and in Fig. 2 of Ref. 9, for any signal from low internal energy radicals that are stable to subsequent dissociation. Instead, the signal in the m/e=55 TOF spectrum shown in Fig. 11 primarily results from dissociative ionization of the acrolein from the H+acrolein dissociation product channel of the vibrationally excited C_3H_5O radicals (solid line fit in Fig. 11 extending from 72 to 88 μs arrival times). The presence of an impurity in the sample makes it impossible to ascertain how much of the C–Cl bond fission $P(E_T)$ should be used when fitting the m/e=55 spectrum, so it was used in its entirety. The m/e=55 TOF spectrum also shows a broad feature peaking near 90 μs. This feature is well fit by assuming that some of the 2-methyleneoxirane fragments produced in the HCl photoelimination channel undergo isomerization and dissociation to $H+C_3H_3O$. More details are given in the supplemental information.[31]

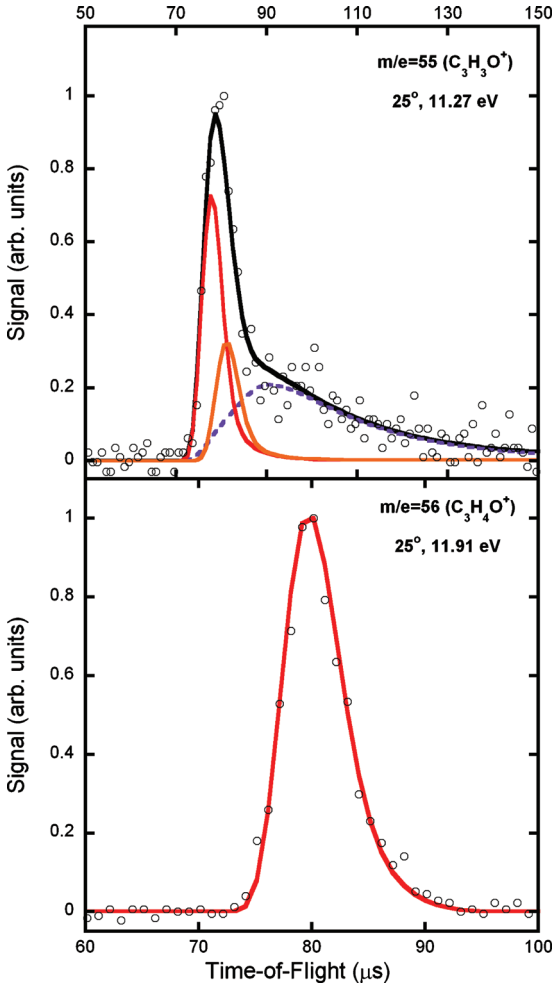

FIG. 11. Time-of-flight spectra corresponding to m/e=55 in the upper frame and m/e=56 in the lower frame. The data points are given by the open circles, the overall fit by the solid black line, the solid, dark gray line represents the fast portion of the m/e=35 $P(E_T)$ in Fig. 8, the solid, light gray line is an impurity in our sample or the sample line. The contribution of the HCl-loss channel is also present in the m/e=55 data and is denoted by the short-dashed gray line. Both spectra were accumulated for 250 000 laser shots and a constant background was subtracted from each.

V. RESULTS ON THE DISSOCIATION PATHWAYS OF C_3H_5O RADICALS

In this section we first briefly review and refine our understanding of the H+acrolein dissociation channel[9] of the nascent C_3H_5O radicals produced in the high-recoil kinetic energy C–Cl bond photofission channel. The radicals dissociate via INT1, a radical intermediate key to the O+allyl reaction. Thus, these experiments on the product channels resulting from the dissociation of these highly vibrationally excited radicals allow us to benchmark theoretical methods for predicting the branching that would result in the bimolecular reaction. Then we describe our experimental results on the dissociation of the radicals to the $HCO+C_2H_4$ and the $H_2CO+C_2H_3$ product channels. The data evidence kinetic energy and angular distributions that are expected for the dissociation of highly rotationally excited radicals via tangential recoil. We then experimentally determine the branching between these radical dissociation product channels by integrating the signal in the TOF spectra and correcting for

the photoionization cross sections of the species detected. This requires careful analysis of the photoionization efficiency curves measured in this experiment with the higher-resolution photoionization spectra of C_2H_4 and vinyl radicals. When the C_3H_5O radicals dissociate to $HCO+C_2H_4$, the HCO is produced in a 1:1 ratio with C_2H_4, whose photoionization cross section is known, so comparison of those relative signals allows us to determine the absolute photoionization cross section of HCO.

A. The dissociation of C_3H_5O radicals to H+acrolein

Our prior study[9] focused on the dissociation of the nascent C_3H_5O radicals to H+acrolein. As this dissociation results in acrolein having essentially the same velocity as the radical that dissociated to H+acrolein, it allows us to assess the internal energies of the radicals that are able to access the H+acrolein product channel. We noted in Ref. 9 that the barrier to the H+acrolein product channel is not the lowest dissociation barrier. Although all of the radicals do dissociate, the lowest internal energy radicals that dissociate must do so via the $HCO+C_2H_4$ product channel and not the H+acrolein product channel. Thus, the m/e=56 TOF spectrum reproduced in Fig. 11, lower frame, from the data presented in Fig. 5 of Ref. 9, is not fit by the entire C–Cl bond fission $P(E_T)$, but rather by a portion of the $P(E_T)$ that excludes the highest recoil kinetic energies. The excluded high E_T portion results in the lowest internal energy radicals; these dissociate to $HCO+C_2H_4$ after surmounting, or by tunneling through, the INT1 → INT4 isomerization barrier. The solid red line in Fig. 12 shows the portion of the $P(E_T)$ used to fit the m/e=56 spectrum shown in the bottom frame of Fig. 12. It is very similar to the dashed line portion of the $P(E_T)$ shown in Fig. 6 of Ref. 9, except for the relative scaling, which does not affect the fit of the TOF spectrum. As Ref. 9 describes in detail, we derived a series of trial $P(E_T)$s to fit the m/e=56 data by weighting each point in the primary C–Cl fission $P(E_T)$ by the fraction of the radicals produced at each E_T that dissociate to H+acrolein. To make the prediction, which depends on the vibrational energy content of the radicals, we used RRKM microcanonical rate constants calculated using the predicted transition states to the H+acrolein, $HCO+C_2H_4$, and $H_2CO+C_2H_3$ product channels shown in Fig. 1. The calculation included only one variable parameter, the fraction that relates the measured C–Cl bond fission recoil kinetic energy, E_T, to the energy partitioned to rotational energy of the radicals. To conserve angular momentum this fraction must be a constant (it depends on the exit impact parameter when the C–Cl bond breaks), $E_{rot}=CE_T$. We entered the constant C as a variable parameter to fit the m/e=56 spectrum. We subtract this rotational energy from the measured internal energy of the radical calculated from Eq. (4) to determine the vibrational energy of the radical at each E_T. When we assumed that the partitioning to rotational energy was $E_{rot}=0.4E_T$, we achieved the excellent fit shown in Fig. 11, bottom. Reference 11 describes the RRKM prediction using MULTIWELL (Refs. 32 and 33) in more detail; it is a refined version of that presented in Ref. 9 to allow for several different conformers of the relevant radical intermediates as well as dissociation to $C_2H_2+H_3CO$. These refinements still give the best fit to the data when we assume $E_{rot}=0.4E_T$. Fitting the acrolein TOF spectrum in this way allows us to estimate the partitioning of the internal energy in the C_3H_5O radical between rotational and vibrational energy. This is key to allowing us to predict the product channel branching from the nascent radicals, as the more energy is partitioned to product rotation the lower the vibrational energy distribution of the dissociating radicals.

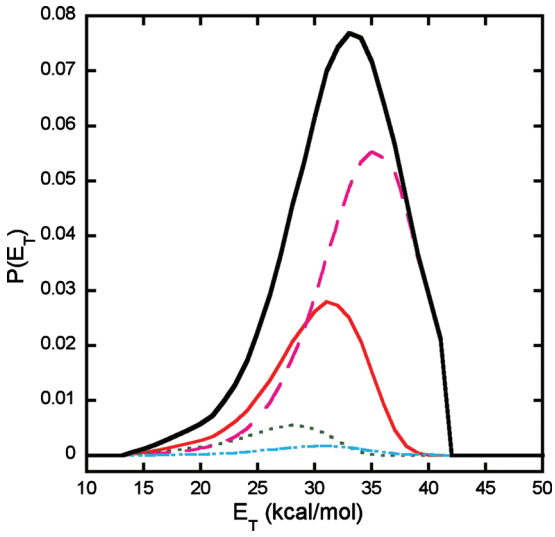

FIG. 12. Division of the 2008 C–Cl bond fission $P(E_T)$ into the predicted portions leading to each of the product channels. The solid black line is the sum of all of the component recoil kinetic energy distributions. The solid red component corresponds to the H+acrolein product channel, and the magenta long-dashed line represents the portion of the primary C–Cl bond fission $P(E_T)$ that gives radicals predicted to dissociate via isomerization to INT4 followed by dissociation to $HCO+C_2H_4$. The predicted contribution of the $H_2CO+C_2H_3$ channel (green dotted line), with the highest barrier and asymptotic energy of the three major dissociation channels, increases for $E_T<35$ kcal/mol. The predicted contribution from all other possible product (dot-dot-dashed line) is predicted to be negligible based on our RRKM calculations and the transition states we identified on the PES. Note that although our simple model predicts that the $HCO+C_2H_4$ component drops sharply near $E_T=42$ kcal/mol (at that E_T the vibrational energy imparted to the radicals drops below the $HCO+C_2H_4$ asymptote), this prediction relies on our very simple model for the partitioning between rotational and vibrational energies.

B. The C–C bond fission products from the dissociation of C_3H_5O radicals

We now turn to the C–C bond fission channels of the nascent C_3H_5O radicals. The transition states on the C_3H_5O PES in Fig. 1 suggest that vibrationally excited INT1 radicals dissociate via three main pathways. Isomerization to INT4 has the lowest barrier, but the isomerization has a tighter transition state than the two direct bond fission dissociation routes, corresponding to H+acrolein and C_2H_3+formaldehyde. Hence, isomerization to INT4, followed by dissociation to $HCO+C_2H_4$, will likely be prevalent for INT1 radicals having relatively low vibrational energies. The two direct bond fission pathways will play an important role for INT1 radicals with larger amounts of vibrational energy. Using the predicted change in microcanonical rate constants for each of these dissociation channels as a function of vi-

brational energy in the radical, we can use the model summarized in the prior section to estimate which regions of the primary C–Cl bond fission channel generate radicals able to access these main dissociation channels. Figure 12 depicts the approximate division of the $P(E_T)$ to the components that result in radicals dissociating to the dominant product channels, $HCO+C_2H_4$, H+acrolein, and $H_2CO+C_2H_3$. The remaining portion is that for dissociation channels predicted to be minor, including $C_2H_2+H_3CO$. For radicals produced in the highest E_T C–Cl bond fission events the $HCO+C_2H_4$ product channel is expected to dominate; the other product channels become more important at lower E_T's that give radicals with higher vibrational energies. Our model, which relies on the statistical rate constants calculated using the transition states calculated on the C_3H_5O PES and our approximate model for the rotational energy imparted to the radicals, predicts the branching fractions between each of the dissociation channels to be 28% for the $H+C_3H_4O$ product channel (10% higher than the experimentally determined value[9]); 60% for the $HCO+C_2H_4$ product channel resulting from the isomerization of INT1 radicals to INT 4; and 6% to C_2H_3+formaldehyde. The remaining 6% is split between dissociation channels predicted to be minor, including $C_2H_2+H_3CO$ and C_2H_5+CO, which rely on traversing high isomerization barriers en route, and INT1 radicals having insufficient vibrational energy to dissociate.

All of the C–C bond fission product TOF spectra presented below are bimodal in nature: this bimodality persists over the entire range of photoionization energies used, which suggests that one fragment produces both peaks in each TOF spectrum. Our analysis below concludes that this bimodal nature results from the dissociation of rotationally excited radicals. When the radicals dissociate, the relative velocity vector imparted to the dissociation products is tangent to the circular orbit, resulting in a strongly forward-backward peaked angular distribution that fits the measured spectra quite well. The high kinetic energy release and forward-backward peaked angular distribution is similar to the dynamics observed for the dissociation of rotationally excited C_2H_4OH radicals to C_2H_4+OH.[34] The high-recoil velocities result from the tangential recoil in the dissociation of the rotating radical; the loose transition state has a small exit barrier, so it does not result in a strong repulsive force between the carbon atoms as the radical dissociates.

1. *The dissociation of* C_3H_5O *radicals to* $HCO+C_2H_4$

Figure 13 shows the TOF spectrum taken at m/e=28 ($C_2H_4^+$). In order to ensure that the signal detected at m/e=28 was due primarily to the photoionization of ethene, we took this spectrum at a VUV photon energy of 11.27 eV, which is well below the appearance energies of CO^+ from HCO [14.6 eV (Ref. 35)], formaldehyde [14.1 eV (Ref. 36)], and ketene [13.6 eV (Ref. 37)]. Although we do not expect any significant branching to the $CO+C_2H_5$ product channel, the photoionization energy used is also below the ionization energy of CO [14 eV (Ref. 37)] and the appearance energy of $C_2H_4^+$ from ethyl radicals [>12.14 eV (Ref. 38)]. (Ethyl radicals would not have enough internal energy to dissociate to C_2H_4+H.[39]) The TOF spectrum at m/e=29 (HCO^+),

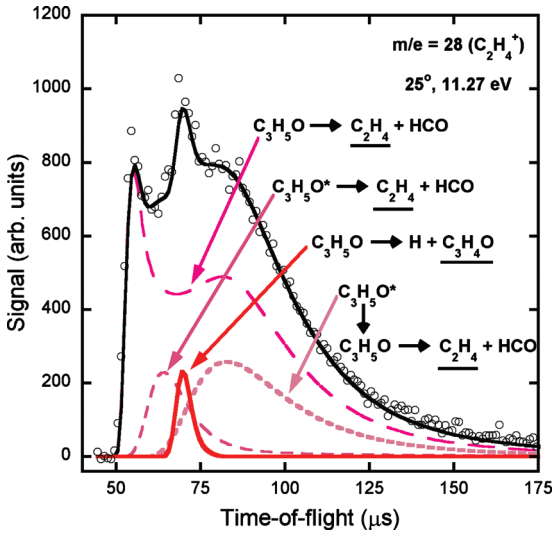

FIG. 13. TOF spectrum of m/e=28 accumulated for 500 000 laser shots; constant background subtraction was used. The open circles are the data points and the solid black line is the overall fit. The fit shown in magenta long-dashed line corresponds to C_2H_4 products formed from ground state C_3H_5O radicals that isomerize from INT1 to INT4 and then dissociate to $HCO+C_2H_4$. The $P(E_T)$ and angular distribution that gave this fit are shown in Fig. 15, top frame, and Fig. 16, respectively. The signal peaking near 70 μs is from dissociative ionization of acrolein; it is fit by the $P(E_T)$ shown in solid red line in Fig. 11. The remaining signal, fit by the short-dashed pink line and the dotted pink line, is assigned to the dissociation of electronically excited state C_3H_5O radicals ($C_3H_5O^*$) formed in the low kinetic energy portion of the C–Cl bond fission $P(E_T)$. They dissociate to $HCO+C_2H_4$ via two competing mechanisms. One imparts significant energy to relative kinetic energy. The $P(E_T)$ in the middle frame of Fig. 15 gives the short dashed line fit peaking near 65 μs. The other imparts less energy to kinetic energy, as shown by the $P(E_T)$ in Fig. 15, bottom. That $P(E_T)$ fits the signal peaking near 85 μs.

shown in Fig. 14, is very similar in shape, as is expected for the momentum-matched partner to C_2H_4. When the C_3H_5O radical dissociates to $HCO+C_2H_4$, the two resulting fragments are of similar mass, and the resulting recoil velocities are nearly equal in magnitude but opposite in direction. If the typical timescale for the dissociation of the C_3H_5O radicals is long with respect to their rotational period, this would result in the velocity imparted to each to be equally distributed in the plane of rotation of the radical. Hence, the TOF spectrum of the ethene fragment would be nearly identical to the TOF spectrum of the HCO fragment. This similarity is indeed what we observe, with one difference. There is a small feature peaking near 70 μs in the m/e=28 TOF that does not appear in the m/e=29 TOF spectrum. This feature is easily assigned to an m/e=28 daughter ion from the dissociative ionization of acrolein at 11.27 eV. To confirm this assignment, we fit the signal with the same partial $P(E_T)$, shown in red in Fig. 12, which fit the m/e=56 TOF spectrum. We also measured the relative intensities of the daughter ions produced from photoionization of a neat acrolein beam at 11.27 eV and found that the strongest dissociative ionization signal was at m/e=28.

The majority of the signal in the m/e=28 and m/e=29 spectra results from the dissociation of C_3H_5O radicals to $HCO+C_2H_4$. To fit the m/e=28 TOF spectrum in Fig. 13, we note that the recoil velocity of the C_2H_4 product in the center-of-mass reference frame is the vector sum of the ve-

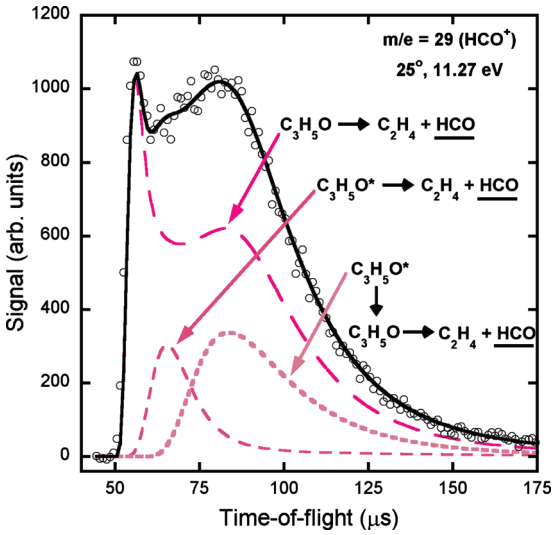

FIG. 14. TOF spectrum of m/e=29 accumulated for 450 000 laser shots. The time-dependent background was subtracted using 125 000 shots with the laser blocked. The open circles are the data points and the solid black line is the overall fit. The fit shown in magenta long-dashed line corresponds to HCO products formed from ground state C_3H_5O radicals that isomerize from INT1 to INT4 and then dissociate to HCO+C_2H_4. The $P(E_T)$ and angular distribution that gave this fit are shown in Fig. 15, top frame, and Fig. 16, respectively. The remaining signal, fit by the short-dashed pink line and the dotted pink line, is assigned to the dissociation of electronically excited state C_3H_5O radicals ($C_3H_5O^*$) formed in the low kinetic energy portion of the C–Cl bond fission $P(E_T)$. They dissociate to HCO+C_2H_4 via two competing mechanisms. One imparts significant energy to relative kinetic energy. The $P(E_T)$ in the middle frame of Fig. 15 gives the short-dashed line fit peaking near 65 μs. The other imparts less energy to kinetic energy, as shown by the $P(E_T)$ in Fig. 15, bottom. That $P(E_T)$ fits the signal peaking near 85 μs.

locity imparted to the C_3H_5O radical in the primary C–Cl bond photofission and the additional velocity imparted to the C_2H_4 fragment as the radical dissociates to HCO+C_2H_4. We begin by fitting the signal from the dissociation of the ground electronic state radicals (90% of the nascent radicals). The portion of the high kinetic energy C–Cl bond photofission $P(E_T)$ that produces radicals expected to dissociate to HCO +C_2H_4 is shown in dashed magenta line in Fig. 12. We use this $P(E_T)$ to generate the velocities of the radicals that dissociate to HCO+C_2H_4, and iteratively vary the energy imparted to the relative velocity between the HCO and C_2H_4 products as each radical dissociates in order to fit the measured TOF spectra at m/e=28 and m/e=29. The $P(E_T)$ shown in the top frame of Fig. 15 gives the best fit to the TOF of the C_2H_4 products; the fit is shown in magenta long-dashed line in Fig. 13. The fit to the momentum-matched HCO cofragments is shown in magenta long-dashed line in Fig. 14. The distribution of kinetic energies imparted to the HCO and C_2H_4 products as the radicals dissociate (Fig. 15, top frame) peaks near 20 kcal/mol with a full-width-at-half-maximum of about 18 kcal/mol. Note that the large magnitude of the relative velocity vector between the HCO and C_2H_4 products is not the result of a large exit barrier, but rather the high rotational energies of the dissociating radicals produced in the dominant C–Cl photofission channel. The fit is relatively insensitive to the velocity of the radical before it dissociates because the velocities imparted to the HCO and C_2H_4 products are large.

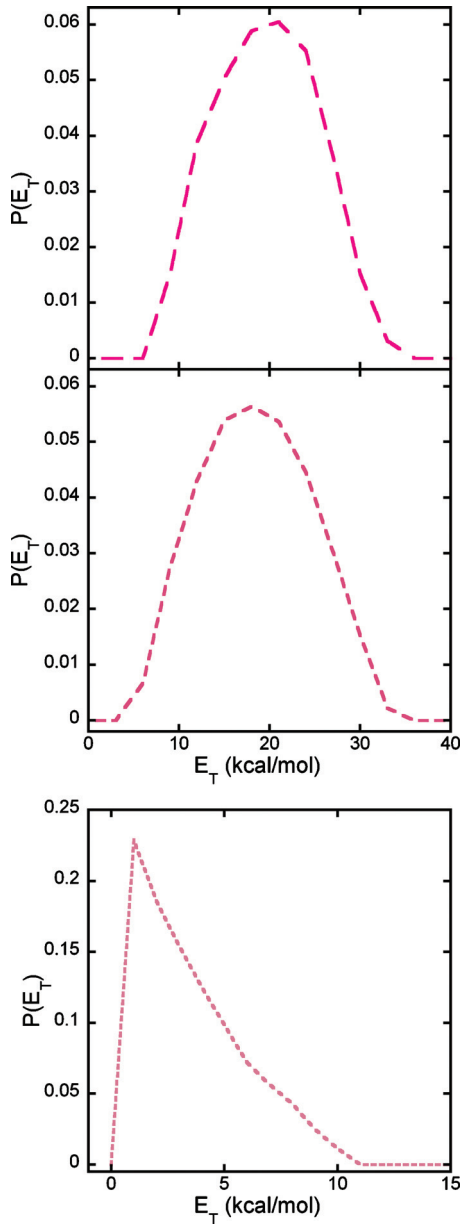

FIG. 15. $P(E_T)$s for the dissociation of ground state C_3H_5O radicals (top frame) and electronically excited state radicals (middle and bottom frames) to HCO+C_2H_4. They are derived from forward convolution fitting of the signal shown in Figs. 13 and 14; the fits in those spectra are shown in the corresponding line types.

When fitting the spectra, one must also specify the angular distribution of the velocity vector of the C_2H_4 and HCO products with respect to the velocity of the radical that dissociated to give these products. Assuming that all azimuthal angles, ϕ, are equally likely (as the plane of the rotation of the radical is evenly distributed in ϕ for a given velocity vector of the dissociating radical), one need only consider the dissociation lifetime compared to the rotational period to determine the necessary angular distribution. If the dissociation lifetime is long with respect to the rotational period of the radical, the recoil direction of the products is uniformly distributed in the plane of rotation (in θ). Thus, the angular distribution is uniform both in θ and in ϕ. To fit the products from the dissociation of the highly rotationally excited ground state radicals, we thus set $I(\theta)=1/\sin\theta$ in the

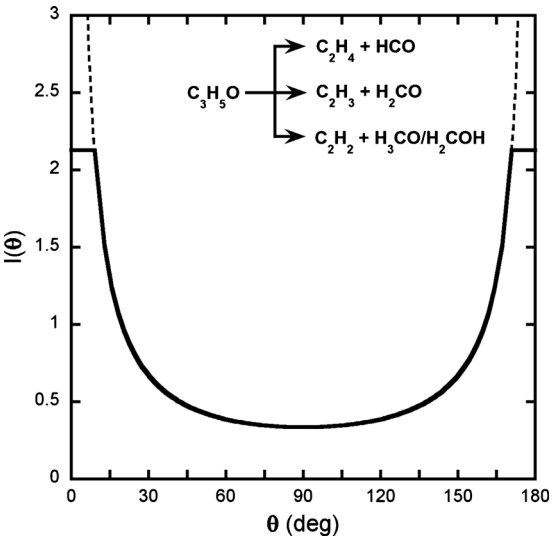

FIG. 16. Angular distribution for the dissociation of ground state C_3H_5O radicals to three product channels: $HCO+C_2H_4$, $H_2CO+C_2H_3$, and $H_3CO+C_2H_2$. The angle θ is the angle between the velocity vector, in the center-of-mass reference frame, of the radical that dissociates and the direction of recoil of the product from that dissociation. This angular distribution is generated by assuming that the dissociation lifetime of the radical is long with respect to its rotational period.

expression $I(\theta)\sin\theta d\theta d\phi$, where the z axis is defined as the direction of the velocity vector of the species that is undergoing secondary dissociation, the C_3H_5O radical, in the center-of-mass reference frame. This $I(\theta)$ blows up at 0° and 180°, so we leveled out the function at $\cos\theta=+/-0.975$ (roughly 13° and 167°). The resulting $I(\theta)$ angular distribution, shown in Fig. 16, is symmetric and strongly forward-backward peaked, as would be expected for the dissociation of a highly rotationally excited C_3H_5O radical. It is identical to the secondary angular distribution used in Ref. 34 after both are appropriately normalized.

We fit the remaining signal in the m/e=28 and m/e=29 spectra to the dissociation of the electronically excited C_3H_5O radicals (labeled as $C_3H_5O^*$ in the figures) to $HCO+C_2H_4$. The initial velocities of the radicals are slower because they are formed in the low kinetic energy portion of the C–Cl bond fission $P(E_T)$ in Fig. 9. The two pairs of fits, shown in short-dashed and dotted lines in Figs. 13 and 14, result from assuming that these radicals dissociated via two competing mechanisms. One mechanism, likely the predissociation of the excited state radicals via a repulsive region of the excited state, imparts substantial relative kinetic energy between the HCO and C_2H_4 products. The $P(E_T)$ shown in the middle frame of Fig. 15 generated the fit shown in short-dashed line. The other mechanism, likely resulting from the internal conversion of the electronically excited radicals to the ground electronic state, imparts much less energy to relative kinetic energy of the $HCO+C_2H_4$ products, as shown by the $P(E_T)$ in the bottom frame of Fig. 15. We fit the HCO and C_2H_4 fragments from the dissociation of electronically excited radicals by assuming that the angular distribution is isotropic; we do not have any empirical estimate of the rotational energy of these radicals.

We briefly considered[9] the possibility that some of the signal with arrival times between 75 and 175 μs in the m/e=28 and 29 TOF spectra might be due to fragments from the dissociation of the momentum-matched fragment in the HCl photoelimination. Some of the 2-methyleneoxirane coproduct to the HCl has enough energy to isomerize to acrolein and dissociate to C_2H_4+CO (Ref. 40) or to $HCO+C_2H_3$. However, the signals in that region of the spectra show that the HCO and C_2H_4 products are generated in a 1:1 ratio, as they would be if they result from C_3H_5O radicals, not from two different dissociation channels of acrolein.

The m/e=29 spectrum in Fig. 14 would not have a contribution from daughter ions of formaldehyde because 11.27 eV is lower than the appearance energy of HCO^+ from H_2CO.[37] The appearance energy of HCO^+ from c-H_2COCH is calculated to be 10.75 or 11.0 eV at the G3//B3LYP level of theory, where the two ionization energies correspond to the production of triplet and singlet CH_2, respectively. This makes dissociative ionization of the CH_2Cl cofragments a possible contributor to the m/e=29 signal. However, the excellent fit to the m/e=29 data shown in Fig. 15 shows that the signal can be all accounted for by the momentum-matched HCO coproducts to C_2H_4 from the dissociation of the C_3H_5O radicals. There is, however, one possible contribution to this spectrum not shown in the fits in Fig. 14. Section V B 5 presents evidence for an unexpected $HCCH+CH_3O$ product channel; HCO^+ may result from the dissociative ionization of CH_3O. This signal would overlap closely the signal fit by the long-dashed and short-dashed lines in Fig. 14, so it might contribute to the signal detected at m/e=29.

2. Photoionization efficiency curves of C_2H_4 and HCO

In addition to fitting the TOF spectra, these data can be used to determine the photoionization efficiency (PIE) curves for the photoionization of C_2H_4 to $C_2H_4^+$ and HCO to HCO^+. These data offer the unique opportunity to derive an absolute photoionization cross section for HCO to HCO^+ as the HCO is formed in a 1:1 ratio with C_2H_4 in the dissociation of C_3H_5O radicals and the absolute photoionization cross section of C_2H_4 is well-characterized.[41–44] Figure 17 compares our C_2H_4 signal integrated from 45 to 60 μs with the latest PIE curve in the literature, convolved with the NSRRC photoionization source bandwidth.[42] We determine the photoionization cross section of HCO at 11.27 eV (averaged over the broad NSRRC bandwidth) by comparing the relative signal at m/e=29 and m/e=28 at 11.27 eV. As the C_2H_4 and HCO neutral products are generated in a 1:1 ratio from the dissociation of C_3H_5O radicals, the ratio of quantum yields or branching fractions $\phi_{HCO}/\phi_{C_2H_4}$ to these two products is 1. It is related to the ratio of integrated signals in the m/e=29 and m/e=28 TOF spectra as shown below,

$$1 = \frac{\phi_{HCO}}{\phi_{C_2H_4}} = \frac{(\text{integrated HCO counts at m/e} = 29)(\text{expected } C_2H_4 \text{ signal})(\sigma_{\text{ion } C_2H_4/C_2H_4^+})}{(\text{integrated } C_2H_4 \text{ counts at m/e} = 28)(\text{expected HCO signal})(\sigma_{\text{ion HCO/HCO}^+})}. \quad (6)$$

(Note, however, that we have not corrected the integrated counts at HCO^+ for the potential contribution from dissociative photoionization of CH_3O discussed in Sec. V B 5.) The expected signal terms correct for the three-dimensional scattering kinematics in the photodissociation and the subsequent unimolecular dissociation of the C_3H_5O radicals, the differing transit times through the ionization region due to the neutral fragment velocities, and the appropriate Jacobian factor. The ratio of the expected signal terms should not deviate from 1 appreciably because the fragments have nearly identical masses and TOF spectra. The integrated counts are discussed in the following paragraph, which leaves the absolute photoionization cross sections as the only unknowns. Hence, having the absolute photoionization cross section of C_2H_4 (to $C_2H_4^+$) allows us to derive the absolute photoionization cross section of HCO (to HCO^+) at 11.27 eV, $\sigma_{\text{ion HCO/HCO}^+}$. The calculation using Eq. (6) sets the absolute scale for the entire HCO PIE curve presented below.

Before delving too far into the PIE curves, a few notes on the construction of our curves are required. The signal-to-noise ratio in most of our individual spectra was not high enough to provide meaningful secondary dissociation fits that could be used to calculate the contribution of the products of interest. We chose to integrate the raw data from 45 to 60 μs (using 65 μs as the end point gave similar results) to avoid any contribution in the m/e=28 spectra due to dissociative ionization of acrolein and any impurities in the beam that generated signal at longer arrival time (these data were taken after the dissociative ionization of a pure acrolein was investigated, and the spectra evidenced some residual impurity signal at longer arrival times). In order to minimize problems with long-time drift, the spectra to be integrated were taken in one continuous block by alternating between the masses of interest (m/e=27–30) while remaining at 11.27 eV. Nine spectra, each accumulated for 50 000 laser shots, were recorded for each mass so that fluctuations in the VUV photon flux, molecular beam intensity, etc. could be averaged out. Due to time limitations, only five spectra at each ionization energy were procured for computing the PIE curves. All spectra are adjusted to compensate for drift in the laser power. Once the raw PIE curve is constructed we put it on an absolute scale by calculating the absolute photoionization cross section at 11.27 eV and scaling all points by this factor, which we calculate by performing a weighted average of σ_{ion} at 11.27 eV using the NSRRC photoionization source bandwidth and the PIE curve of Cool *et al.*[42] In a similar vein, we convolved the NSRRC VUV bandwidth with the PIE curve of Cool *et al.* to compensate for the spectrally narrow photoionization source they used.

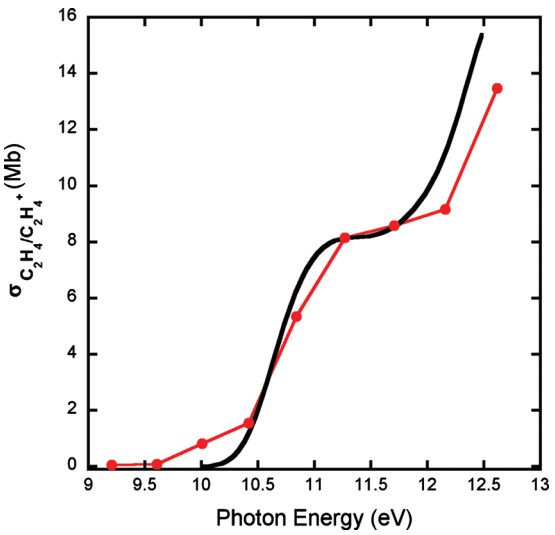

FIG. 17. Photoionization efficiency curve of m/e=28, scaled to 8.14 Mb at 11.27 eV. The black line denotes the $C_2H_4/C_2H_4^+$ PIE curve of Cool *et al.* (Ref. 42) convolved with the NSRRC photonization source bandwidth to provide a more equitable comparison. Reference 42 only shows a portion of the PIE curve; the higher energy region provided to us by Cool *et al.* is given in the supplementary document. The red line with data shown in solid circles is the low resolution PIE curve taken in the present work. The data points show the integrated signal in the m/e=28 TOF spectra from 45 to 60 μs. It is scaled to fit the PIE curve of Cool *et al.*, with the latter's absolute scale averaged over the NSRRC VUV photoionization source bandwidth.

Returning to the PIE curves, starting with Fig. 17, we see that our m/e=28 PIE curve is an excellent match to the C_2H_4 PIE curve of Cool *et al.* The slopes from 10.5 to 11 eV and 12 to 12.5 eV are similar, as is the presence of a shelf from 11 to 11.5 eV. The onset in our data occurs about 0.5 eV lower in energy, indicating that the C_2H_4 fragments in our experiment have a higher average vibrational energy. Application of Eq. (6) at 11.27 eV, but without correcting the integrated signal at m/e=29 for the potential dissociative ionization of the CH_3O cofragment to the HCCH product channel discussed in Sec. V B 5, yields an absolute photoionization cross section of 11.6 ± 0.9 Mb for HCO $\rightarrow HCO^+$. These error bars represent a 95% confidence interval reflecting only the reproducibility of the relative signals. To estimate the systematic error due to a possible contribution to the HCO^+ signal from dissociative ionization of CH_3O, one may recalculate the cross section assuming that the partial photoionization cross section of HCO to HCO^+ is similar to that of CH_3O to CHO^+. Then, correcting the observed m/e=29 signal for this contribution using the product branching fraction for the HCCH product channel in Eq. (8) gives an HCO photoionization cross section of 8.8 Mb. Thus, the error bars in our determination of the HCO photoionization cross section are larger and asymmetric+1/−3 Mb at 11.27 eV. From this σ_{ion} we can put our entire PIE curve on an absolute scale. To the best of our knowledge, the result shown in Fig. 18 is the first PIE curve of HCO having absolute photoionization cross sections. We note though that the

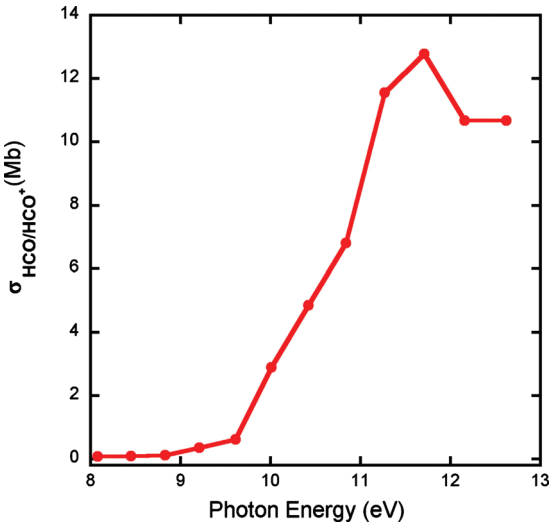

FIG. 18. PIE spectrum of the m/e=29 signal assigned to HCO. It is placed on an absolute scale by multiplying the absolute photoionization cross section of C_2H_4 at 11.27 eV by the ratio of the respective integrals of the m/e=29 and m/e=28 TOF spectra from 45 to 60 μs. The m/e=29 integrated signal is not corrected for a possible contribution from the dissociative ionization of CH_3O. This possible systematic error increases the uncertainty in the derived cross sections to roughly +10%/−30%. The integrated signal at m/e=28 and m/e=29 was taken independently of the PIE spectra, alternating between m/e=28 and m/e=29 at 11.27 eV in order to average out fluctuations in the laser power, etc. We assume that the photon flux at the NSRRC did not change appreciably in the range from 9 to 12 eV, but the drop in cross section at energies of >12 eV in the figure may be due to not correcting for a reduced photon flux, as noted in the text.

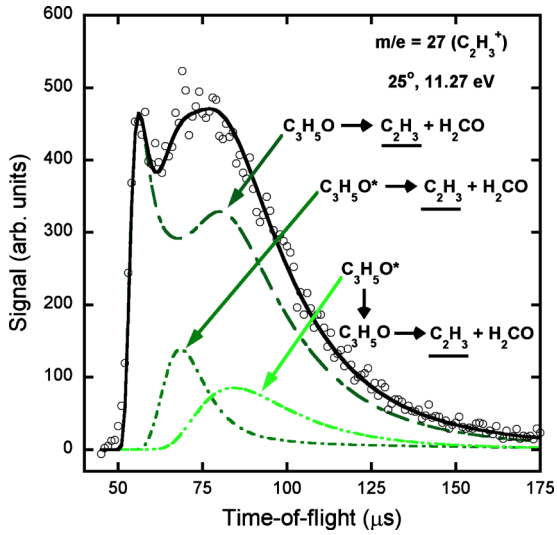

FIG. 19. Time-of-flight spectrum of m/e=27 accumulated for 500 000 laser shots and having constant background subtraction. The open circles are the data points and the solid black line is the overall fit. The fit shown in green long-short-long dashed line corresponds to C_2H_3 products formed from ground state C_3H_5O radicals that dissociate directly from INT1 to $H_2CO + C_2H_3$ (the other direct bond fission channel from this intermediate is H + acrolein). The $P(E_T)$ and angular distribution that gave this fit are shown in Fig. 21, top frame, and Fig. 16, respectively. [We assume the radicals have initial velocities determined by the $P(E_T)$ in green dotted line in Fig. 11, but changes to that do not substantially alter the fit.] The remaining signal, fit by the dot-dashed green line and the dot-dot-dashed green line, is assigned to the dissociation of electronically excited state C_3H_5O radicals ($C_3H_5O^*$) formed in the low kinetic energy portion of the C–Cl bond fission $P(E_T)$. They dissociate to $H_2CO + C_2H_3$ via two competing mechanisms. One imparts significant energy to relative kinetic energy. The $P(E_T)$ in the middle frame of Fig. 21 gives the dot-dashed green line fit peaking near 65 μs. The other imparts less energy to kinetic energy, as shown by the $P(E_T)$ in Fig. 21, bottom. That $P(E_T)$ fits the signal peaking near 85 μs.

contribution from dissociative ionization of H_3CO to HCO^+ has not been subtracted from these data; although we could do so approximately by assuming that the contribution from this source is proportional to its neutral branching fraction relative to $HCO + C_2H_4$ across the PIE spectrum, we prefer to leave this correction to after such time as the PIE curve of CH_3O is measured. Finally, the apparent reduction in cross section above 12 eV cannot be due to dissociative ionization (as the appearance energy of CO^+ from HCO is much higher); it may be due to the fact that this spectrum is uncorrected for a possible change in the photon flux as the photoionization source was tuned. A drop in photon flux at energies greater than 12 eV also explains why the measured C_2H_4 PIE curve in Fig. 17 falls below the calibration curve of Cool *et al.* for photon energies greater than 12 eV. The HCO photoionization onset between 9 and 9.5 eV is substantially higher in energy than the calculated adiabatic ionization energy of 8.1–8.5 eV, because the equilibrium geometry of the HCO cation differs from that of neutral HCO. Dyke *et al.*[45] measured the photoelectron spectra of HCO and determined the vertical IE to be 9.3 eV, which is in close agreement with our onset. However, some caution must be taken in comparing our experiments with their work because the $F + H_2CO$ reaction they used to generate HCO resulted in formyl radicals that only showed one vibrational progression, the H–C–O bend.

A qualitative comparison between our m/e=29 PIE curve assigned to HCO and the C_2H_5 PIE curve of Wang *et al.*[46] shows that they are, as expected, quite different. The onset of the latter is about 8.5 eV and exhibits a plateau from 9 to 10.5 eV, whereas Fig. 18 shows that our m/e=29 PIE curve has a higher energy onset and does not plateau until above 11 eV. These differences confirm that ionization of ethyl radicals does not constitute a significant fraction of our m/e=29 signal, and supports our assessment that mass 29 fragments are HCO and not C_2H_5.

3. *The dissociation of* C_3H_5O *radicals to* $H_2CO + C_2H_3$

The third major product channel originating from the unimolecular dissociation of INT1 C_3H_5O radicals is $C_2H_3 + H_2CO$. Figure 19 shows the TOF spectrum taken at m/e=27 ($C_2H_3^+$) and Fig. 20 displays the TOF spectrum taken at m/e=30 (H_2CO^+). No neutral C–Cl fission photoproduct may dissociatively ionize to m/e=30 (the calculated appearance energy of H_2CO^+ from c-H_2COCH is 14.1 eV), so all the signal in the m/e=30 spectrum is assigned to the dissociation of C_3H_5O radicals to $H_2CO + C_2H_3$. Production of m/e=27 ions via dissociative ionization of c-$HCOCH_2$ is unlikely, and dissociative ionization of acrolein to yield m/e=27 ions is minor (similar to that of m/e=29 at 11.27 eV) and does not appear to give an appreciable contribution to the m/e=27 spectrum. Again, we fit the majority of the signal in both spectra by assuming that ground state radicals generated in a portion of the high kinetic energy C–Cl bond fission are formed vibrationally and rotationally excited and can dissociate to $H_2CO + C_2H_3$. The fit shown in long-short-

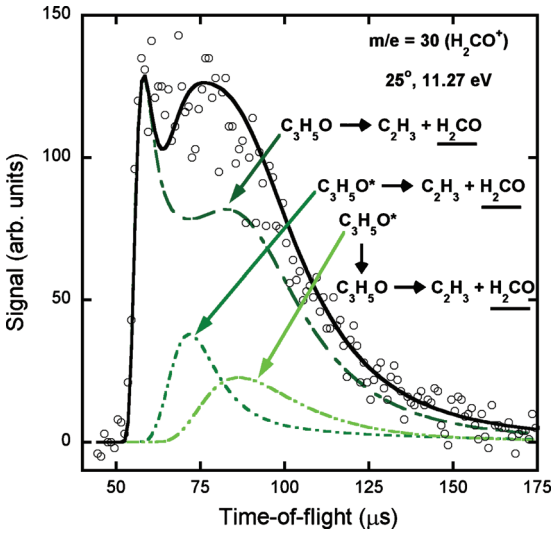

FIG. 20. Time-of-flight spectrum of m/e=30, accumulated for 500 000 laser shots and with constant background subtracted. The open circles correspond to the data and the solid black line is the overall fit. The fit shown in green long-short-long dashed line corresponds to H_2CO products formed from ground state C_3H_5O radicals that dissociate directly from INT1 to $H_2CO+C_2H_3$ (the other direct bond fission channel from this intermediate is H+acrolein). The $P(E_T)$ and angular distribution that gave this fit are shown in Fig. 21, top frame, and Fig. 16, respectively. The remaining signal, fit by the dot-dashed green line and the dot-dot-dashed green line, is assigned to the dissociation of electronically excited state C_3H_5O radicals ($C_3H_5O^*$) formed in the low kinetic energy portion of the C–Cl bond fission $P(E_T)$. They dissociate to $H_2CO+C_2H_3$ via two competing mechanisms. One imparts significant energy to relative kinetic energy. The $P(E_T)$ in the middle frame of Fig. 21 gives the dot-dashed green line fit peaking near 65 μs. The other imparts less energy to kinetic energy, as shown by the $P(E_T)$ in Fig. 21, bottom. That $P(E_T)$ fits the signal peaking near 85 μs.

long dashed line results from a high kinetic energy release, shown in the top frame of Fig. 21, between the H_2CO and C_2H_3 products and a strongly forward-backward peaked angular distribution shown in Fig. 16. The high kinetic energy release, peaking near 18 kcal/mol, is not due to repulsive forces in the exit channel, but rather to the tangential recoil of the fragments from a radical with high rotational energy. The remaining signal in both spectra is fit to the dissociation products from electronically excited radicals formed in the low kinetic energy C–Cl bond fission channel. The $P(E_T)$s that gave the best fit are similar to those that fit the dissociation of electronically excited radicals to $HCO+C_2H_4$. Similar to the HCO/C_2H_4 spectra, the C_2H_3/H_2CO fits suggest two competing mechanisms for the dissociation of electronically excited radicals to $H_2CO+C_2H_3$, one that imparts significant energy to relative translation (Fig. 21, middle frame) and one that imparts little energy to kinetic energy (Fig. 21, bottom frame). The angular distribution of those dissociation processes is taken as isotropic.

4. Photoionization efficiency curves of C_2H_3 and H_2CO

Our data can be used to determine the photoionization efficiency curves for the photoionization of C_2H_3 to $C_2H_3^+$ and H_2CO to H_2CO^+. Comparing our vinyl PIE curve with the high resolution photoionization spectrum measured by Taatjes,[47] convolved with the NSRRC bandwidth, allows us

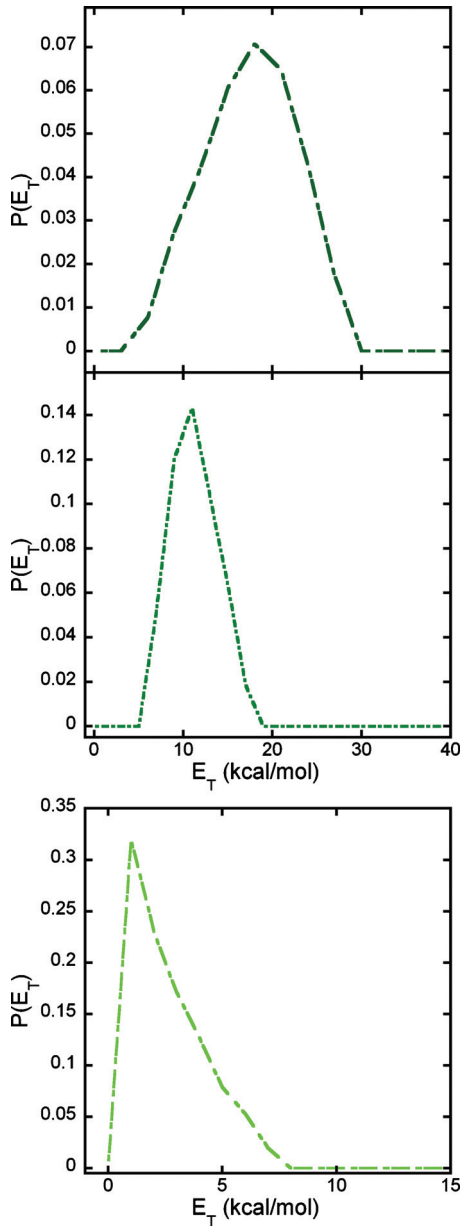

FIG. 21. $P(E_T)$s for the dissociation of ground state C_3H_5O radicals (top frame) and electronically excited state radicals (middle and bottom frame) to $H_2CO+C_2H_3$. They are derived from forward convolution fitting of the signal shown in Figs. 19 and 20; the fits in those spectra are shown in the corresponding line types.

to put our measured spectrum on an absolute scale. We can then use the relative signal levels at m/e=30 from H_2CO and m/e=27 from vinyl radicals to derive an absolute photoionization cross section for H_2CO at 11.27 eV, averaged over the NSRRC bandwidth. A comparison of our vinyl PIE curve with those of Neumark and co-workers[48] and Taatjes and co-workers also helps establish which of the prior measurements are best if the vinyl radicals being detected are not highly vibrationally excited.

Figure 22 shows how we calibrated the low-resolution PIE curve of vinyl radicals using the photoionization spectrum of vinyl radicals measured by Taatjes.[47] The data points are our measurements, and they are plotted with the photoionization spectrum of Taatjes and co-workers, but with the

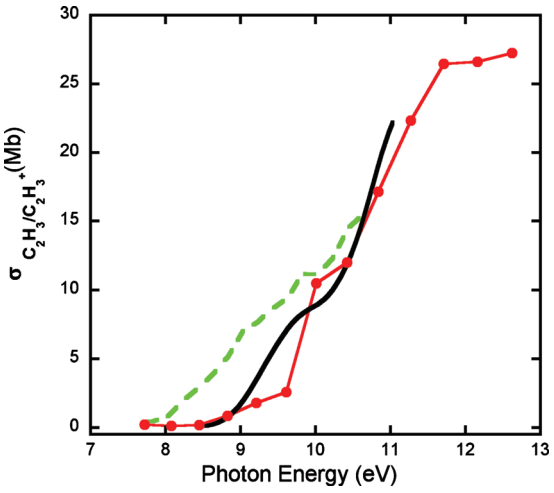

FIG. 22. Photoionization efficiency curves of C_2H_3. Our spectrum, shown in solid circles connected by red solid line, is scaled to 12.0 Mb at 10.43 eV to fit it to the published photoionization spectrum of vinyl radicals in Ref. 47. The solid black line shows the photoionization spectrum of vinyl radicals determined by Taatjes (Ref. 47); we have convoluted that spectrum with the NSRRC VUV bandwidth for comparison with our spectrum. The gray dashed line corresponds to the C_2H_3 PIE curve of Neumark and co-workers (Ref. 48); we have added a correction of −0.2 eV to correct the published spectrum for a recalibration of the beamline calculator subsequent to that work.

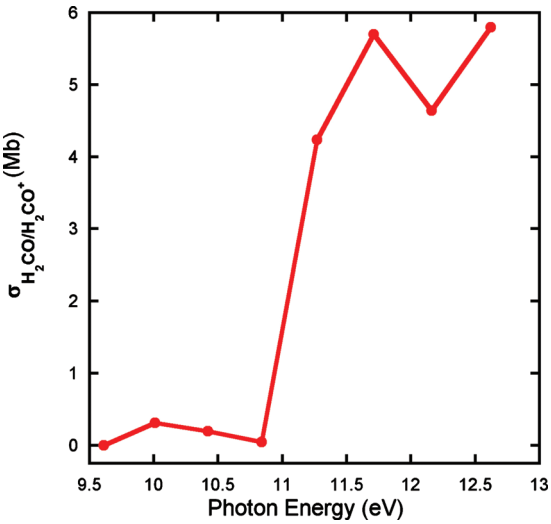

FIG. 23. PIE curve of H_2CO from 9.5 to 12.75 eV. The absolute photoionization cross section was determined by comparison of the signal intensities at m/e=30 and m/e=27 at 11.27 eV, which set that cross section at 4.2 ± 0.5 Mb (averaged over the NSRRC bandwidth).

latter convolved with the NSRRC bandwidth. We scaled our PIE curve to that of Taatjes and co-workers by setting them equal at 10.43 eV. That allowed us to put our PIE curve on an absolute scale. At 11.27 eV, the resulting photoionization cross section is 22.3 Mb (an average over the NSRRC VUV bandwidth). Figure 22 also shows a comparison with the vinyl PIE curve measured by Neumark and co-workers,[48] where we have shifted the VUV photon energies reported in Ref. 48 by −0.2 eV to compensate for a miscalibrated beamline calculator.[49] Our curve matches that of Taatjes and co-workers fairly well at the onset and above 9.75 eV. Our higher photon energy data show that the curve starts to level off above 11.75 eV (corresponding to 27 Mb). In contrast, the PIE curve of C_2H_3 measured by Neumark and co-workers displays a much earlier onset, near 8 eV; this is a roughly 0.75 eV lower energy onset than the other two. The vinyl radicals in that study were generated from the 193 nm photodissociation of vinyl chloride, and C_2H_3 is known to have a nonvertical ionization due to formation of a lower energy (as compared to the classical Y structure) bridged-acetylene structure.[50,51] Thus, we presume that the apparent earlier onset in the data of Neumark and co-workers is due to hot bands in the photoionization spectrum.

Figure 23 displays our measured PIE curve for H_2CO measured at m/e=30 with the broad NSRRC photoionization source. The sharp onset at 10.75 eV matches well with those reported in literature.[37] After the onset it quickly rises to a maximum of 5.75 Mb by 11.75 eV, which is still well below the threshold of dissociative ionization to HCO^++H. We used the relative signals at 11.27 eV in the m/e=27 and m/e=30 TOF spectra to put our H_2CO PIE curve on an absolute scale [using the analog of Eq. (6)]. The relative signal levels show that H_2CO has a much lower photoionization cross section than its momentum-matched partner C_2H_3, being only 4.2 ± 0.5 Mb at 11.27 eV. Ten spectra at each mass-to-charge ratio, each consisting of 50 000 laser shots, were accumulated at 11.27 eV to determine the relative signal levels at $C_2H_3^+$ and H_2CO^+; we used 22.3 Mb as the bandwidth-averaged photoionization cross section of vinyl radicals at 11.27 eV to convert the relative signal levels to a photoionization cross section for H_2CO.

5. The dissociation of C_3H_5O *radicals to* HCCH + H_3CO/H_2COH

Although they are not shown in Fig. 1, there are at least two acetylene-forming channels on the O(^{3}P)+allyl PES. They are detailed in Ref. 11. One is the result of a C–O bond cleavage from INT14; the resulting cofragment is H_3CO. The second HCCH channel stems from one of the enolic intermediates, INT22; the HCCH cofragment is H_2COH. Although the branching to the acetylene product channels is predicted to be small, only about 2% shared between the remaining product channels, the m/e=26 data in Fig. 24 show substantial signal and a similar form to the C–C bond fission TOF spectra discussed above. Namely, there is a sharp onset leading to a narrow peak at about 50 μs followed by a slower, broader peak near 70 μs. This spectrum cannot be the result of dissociative ionization of C_2H_4 because the appearance energy of $C_2H_2^+$ from ethene is above 13.3 eV.[37] G3//B3LYP calculations place the appearance energy of $HCCH^+$ from C_2H_3 at 12.9 eV, which eliminates dissociative ionization of vinyl radicals. Thus, we assign this signal to acetylene from the HCCH+H_3CO/H_2COH dissociation channels of the rotationally excited C_3H_5O radicals.

Neither of the cofragments to HCCH were detected at m/e=31. This is not surprising as it is well known that H_3CO radicals readily undergo dissociative ionization to HCO^++H_2.[52,53] Thus, the m/e=29 spectrum shown in Fig. 14 likely includes a contribution not only from HCO but also from dissociative ionization of H_3CO radicals, as m/e=29 dominates the mass spectrum of both radicals at 11.27 eV

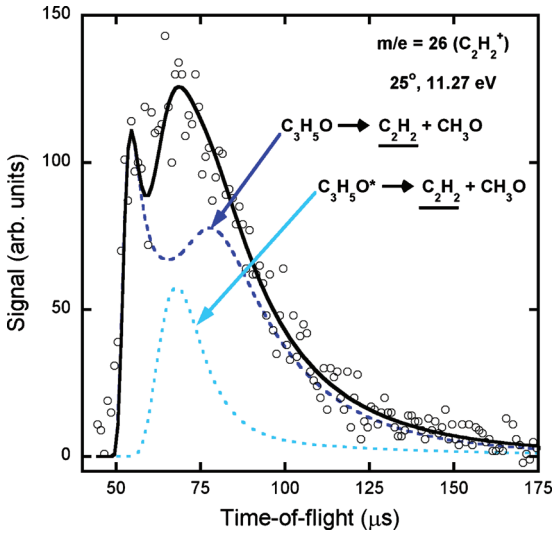

FIG. 24. Time-of-flight spectrum of m/e=26, accumulated for 500 000 laser shots and having constant background subtraction. Open circles represent the data points and the solid black line is the overall fit. The dashed dark-gray line (blue in color) fits the signal assigned to the dissociation of a ground electronic state radical intermediate on the $O(^3P)$+allyl PES, most likely INT14 or INT22, to HCCH+H_3CO/H_2COH. The fit is generated from the $P(E_T)$ in Fig. 25, top frame, and the angular distribution in Fig. 16, using initial radical velocities calculated from the dot-dot-dashed portion of the C–Cl bond fission $P(E_T)$ in Fig. 12. The light-blue dashed line shows the fit of the signal assigned to C_2H_2 products from the dissociation of electronically excited state C_3H_5O radicals (denoted $C_3H_5O^*$ in the figure) produced in the low kinetic energy portion of the C–Cl bond fission $P(E_T)$. The distribution of recoil kinetic energies between the C_2H_2 and H_3CO products that fit this signal is shown in the lower frame in Fig. 25.

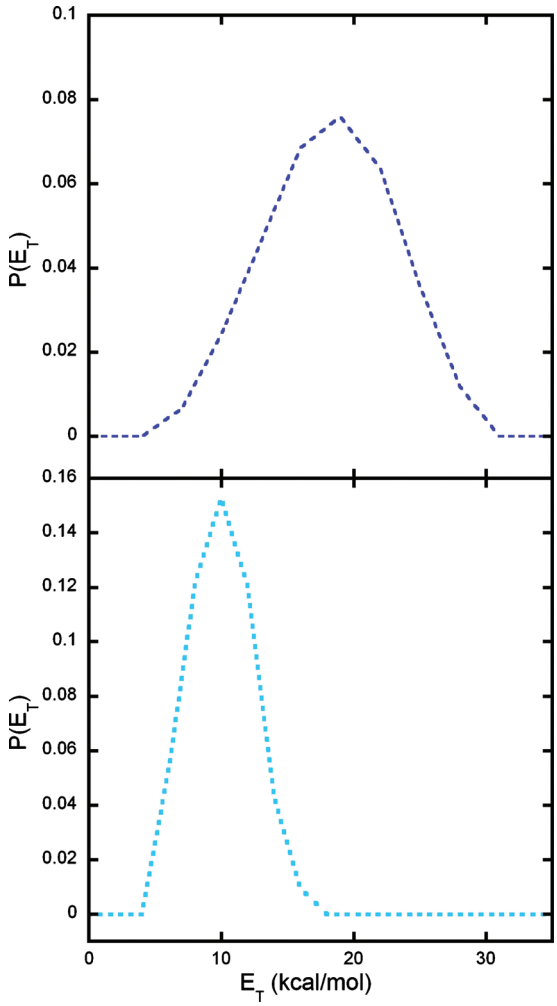

FIG. 25. $P(E_T)$s for the dissociation of a radical intermediate to HCCH +H_3CO/H_2COH. The top frame shows the $P(E_T)$ for the dissociation of a ground electronic state intermediate on the $O(^3P)$+allyl PES; it is derived from fitting the bimodal portion of the signal in Fig. 24 with the angular distribution shown in Fig. 16. The lower frame shows the recoil kinetic energy imparted during dissociation of electronically excited radicals, formed in the low recoil kinetic energy C–Cl bond fission events, to HCCH+H_3CO/H_2COH. The corresponding fit in Fig. 24 peaks near 68 μs.

and below. The velocity distribution of the momentum-matched cofragments of HCCH is calculated to be similar to the signal depicted in long- and short-dashed lines in Fig. 14, so it cannot be separately identified in those spectra.

We fit the HCCH product TOF with a dominant component assigned to the dissociation of ground state radicals, shown in dark-blue dashed line in Fig. 24, and a minor component from the dissociation of excited state radicals, shown in light-blue dashed line in Fig. 24. The corresponding $P(E_T)$s are depicted in the top and bottom frames of Fig. 25. Again, the products from the dissociation of ground state radicals are strongly forward-backward peaked (Fig. 16), and the angular distribution of the products from the dissociation of excited state radicals is assumed to be isotropic. The distribution of recoil kinetic energies imparted to the HCCH +H_3CO/H_2COH products, depicted in the top frame of Fig. 25, is very similar to those used to fit the HCO+C_2H_4 and the $H_2CO+C_2H_3$ products from the dissociation of ground state C_3H_5O radicals. This similarity is expected if the kinetic energy release results from tangential recoil as the rotationally excited radicals undergo C–C bond cleavage (see Sec. VI).

C. Product branching ratios from ground state C_3H_5O radicals

Our experiments detected four major product channels from the unimolecular dissociation of ground state C_3H_5O radicals: H+acrolein, HCO+C_2H_4, $H_2CO+C_2H_3$, and HCCH+H_3CO/H_2COH. There was negligible branching to the most exothermic product channel, C_2H_5+CO. In this section we report the experimentally measured branching fractions to each of these channels. We compare the measured branching with a simple statistical prediction using RRKM theory and the relevant transition states on the global C_3H_5O ground state PES. Although the RRKM predictions are in qualitative agreement with the measured branching for the first three of these product channels, and with the negligible branching to the C_2H_5+CO channel, the measured branching to the HCCH+H_3CO/H_2COH product channel is much larger than that predicted by the theoretical model.

We determine the branching ratios between the different C–C bond fission channels of ground state C_3H_5O radicals by integrating the signal in the TOF spectra as described below and correcting for the ionization cross sections of the detected species. To determine the HCO+C_2H_4:H_2CO +C_2H_3 product branching ratio, we integrated the signal under the fits for the products from ground state radicals shown in Fig. 19 (for m/e=27) and Fig. 13 (for m/e=28). (In this

way, we excluded the signal at m/e=28 from dissociative ionization of acrolein. We also exclude the signal from the dissociation of electronically excited radicals, although including that signal does not appreciably affect the ratios below). Equation (7) gives our experimental branching ratio determination,

$$\frac{\phi_{HCO+C_2H_4}}{\phi_{H_2CO+C_2H_3}} = \frac{(\text{integrated } C_2H_4 \text{ counts at m/e} = 28)}{(\text{integrated } C_2H_3 \text{ counts at m/e} = 27)} \times \frac{(\text{expected } C_2H_3 \text{ signal})}{(\text{expected } C_2H_4 \text{ signal})} \times \frac{(\sigma_{\text{ion } C_2H_3/C_2H_3^+})}{(\sigma_{\text{ion } C_2H_4/C_2H_4^+})} = \frac{(2666)}{(1524)} \times 1.07 \times \frac{(22.3 \text{ Mb})}{(8.14 \text{ Mb})} = 4.54 \pm 0.49. \quad (7)$$

The integrated counts are the average number of counts in 50 000 laser shots from nine background subtracted spectra taken by alternating between the relevant mass-to-charge ratios (including a normalization for laser power). We integrate the total signal from 40 to 100 μs (total neutral+ion flight time, as the ion flight time difference is only a microsecond) and retain the fraction of the integrated counts due to products from ground state radicals. Because the TOF spectra of these components in the m/e=27 and m/e=28 spectra are nearly identical, the ratio of expected signals is essentially 1. (The "expected signal" normally accounts for differing kinematics, transit time through the ionizer, and Jacobian factors.) Thus, our data give the experimental $HCO+C_2H_4$:$H_2CO+C_2H_3$ product branching ratio to be 4.5 ± 0.5 (95% confidence interval). The confidence interval only represents the reproducibility of the integrated signals. The absolute ionization cross sections used in this determination are subject to errors of roughly 20%.

To determine the $HCO+C_2H_4$:$HCCH+H_3CO/H_2COH$ product branching ratio, we integrated the signal under the fits for the products from ground state radicals shown in Fig. 24 (for m/e=26) and Fig. 13 (for m/e=28). As before, we only retain the signal due to the dissociation of ground state radicals, and correct the signal at these two mass-to-charge ratios by the relative ionization cross sections of ethene and acetylene at 11.27 eV. As the NSRRC photoionization source bandwidth is broad and the IE for acetylene is 11.4 eV, we did not attempt to calculate the bandwidth averaged photoionization cross section of acetylene from the high resolution spectra in the literature.[42] Instead, we determined the ratio of cross sections needed in Eq. (8) below by measuring the total signal detected from neat beams of ethene and acetylene at the NSRRC beamline in the same week that we measured the relative signal in the TOF spectra presented in this paper,

$$\frac{\phi_{HCO+C_2H_4}}{\phi_{HCCH+H_3CO}} = \frac{(\text{integrated } C_2H_4 \text{ counts at m/e} = 28)}{(\text{integrated HCCH counts at m/e} = 26)} \times \frac{(\text{expected HCCH signal})}{(\text{expected } C_2H_4 \text{ singal})} \times \frac{(\sigma_{\text{ion HCCH/HCCH}^+})}{\sigma_{\text{ion } C_2H_4/C_2H_4^+}} = \frac{(2666)}{(409)} \times (1.05) \times \frac{(4.15 \text{ Mb})}{(8.14 \text{ Mb})} = 3.10 \pm 0.27. \quad (8)$$

Note that the photoionization cross section for acetylene is averaged over the broad NSRRC bandwidth, so even when it is centered near 11.27 eV (and this is a nominal energy from the beamline calculator) we note that a substantial fraction of the photons have energy exceeding 11.4 eV. The resulting branching to the $HCCH+H_3CO/H_2COH$ channel is surprisingly large, comparable to the $H_2CO+C_2H_3$ product channel. This is in contrast to the statistical estimate from our RRKM-based model using MULTIWELL; that predicts less than 2%. We identified several previously unconsidered routes, via isomerization from INT2 and INT1 (one through INT22 and one through INT14 depicted in Fig. 1), to try to discover a route to this product channel that would make a large contribution to the product branching, but the transition states on the possible routes we considered were too tight or at too high an energy. Thus, we are unable to understand the significant branching to this product channel with a statistical model for the dynamics and the transition states we were able to characterize computationally. We note that although most of the TOF data in this paper were reproduced in three separate trips to the NSRRC, it was only during the third trip that we sought to detect signal at m/e=26. Thus, our branching to this product channel is subject to being reproduced by other groups.

Our prior work[9] reported an experimental branching fraction of 18% to the H+acrolein channel from the ground state radicals produced in the high kinetic energy C–Cl bond photofission events. Presuming that the $HCO+C_2H_4$, $H_2CO+C_2H_3$, and $HCCH+H_3CO/H_2COH$ product channels make up the rest of the product branching, 82%, we can use the product branching ratios determined above to derive experimental values for the absolute branching fractions to these product channels. They are 53% for the $HCO+C_2H_4$ product channel, 12% to the C_2H_3+formaldehyde product channel, and 17% to the $HCCH+H_3CO/H_2COH$ product channels. Our statistical calculations with the transition states depicted in Fig. 1 predict branching fractions of 28% for the $H+C_3H_4O$ product channel (10% higher than the experimentally determined value[9]); 60% for the $HCO+C_2H_4$ product channel resulting from the isomerization of INT1 radicals to INT 4; and 6% to C_2H_3+formaldehyde. The remaining 6% is split between dissociation channels predicted to be minor, including $C_2H_2+H_3CO$ and C_2H_5+CO, which rely on traversing high isomerization barriers en route, and INT1 radicals that have insufficient vibrational energy to dissociate to $HCO+C_2H_4$ (using the empirical estimate that $E_{rot}=0.4\ E_T$).

Neither the experiments nor the statistical predictions evidence substantial branching to the C_2H_5+CO product channel. The statistical predictions for the product branching are in reasonable agreement with the experiment, with the exception of the branching to acetylene product. Note that these branching ratios result from the radical intermediate in the O+allyl bimolecular reaction when the O atom adds to an end C atom, and for internal energies in this intermediate which are far lower than that for the bimolecular reaction. While they offer an important test of theoretical predictions based on the calculated potential energy surface for the bimolecular reaction, they should not be compared directly to the thermal product branching ratios measured in a bulk kinetics experiment on the bimolecular reaction.

One potential source of error in the experimental branching ratio determinations is as follows. To detect HCO and C_2H_4 products from the $HCO+C_2H_4$ dissociation channel, the radical must dissociate before it flies out of the viewing volume of our detector. The transit time through this viewing volume is $1-2$ μs. This is not usually a source of significant error, as typical microcanonical rate constants for bond fission reactions exceed 10^9 s^{-1} at energies even 0.5 kcal/mol above the relevant barrier. However, for the $HCO+C_2H_4$ dissociation pathway our RRKM calculations combined with the vibrational energy distribution of the ground state radicals derived from our Cl TOF data and the estimated partitioning to rotational energy equal to $0.4E_T$ suggest that a substantial fraction of the radicals have vibrational energies below the barrier for INT1 to isomerize to INT4, from which they dissociate to $HCO+C_2H_4$. If the lifetime for tunneling through this isomerization barrier is short, then the radicals dissociate to $HCO+C_2H_4$ while they are within the viewing volume of the detector. However, for radicals with an isomerization lifetime greater than a microsecond or two, the radicals can fly out of the viewing volume of the detector and, although they dissociate to $HCO+C_2H_4$, will not be detected in our TOF spectra. Hence, we are insensitive to any products from radicals with dissociation lifetimes longer than a microsecond or two. Although one-dimensional Eckart tunneling estimates through the INT1 → INT4 isomerization barrier are relatively fast (as it involves primarily H atom motion), some of the yield of this product channel may not be observed in our experiments.

VI. DISCUSSION

Reactions involving open-shell species tend to be complex, especially when oxygen atoms are involved. Reactions of hydrocarbons with $O(^1D)$ can proceed via an insertion mechanism,[54] whereas $O(^3P)$ reactions tend to proceed via two distinct mechanisms, addition/elimination or direct abstraction. One strength of our experiments lies in directly probing the addition/elimination pathways of the O+allyl reaction by generating a particular radical intermediate photolytically. Starting with only one intermediate allowed us to make substantial progress in a very complicated system that had otherwise proved intractable for detailed dynamical studies. The complexity of these atomic oxygen and hydrocarbon systems is exemplified by the experiments in this work, which can access a myriad of C–H and C–C bond fission product channels because many of the barrier heights are energetically proximal. Hence, small changes in the barrier heights predicted from *ab initio* electronic structure calculations may result in large changes in the expected product branching. These experiments offer valuable comparisons for benchmarking *ab initio* studies of transition states in open-shell systems.

Because the barriers to the two competing bond fission channels and the INT1 → INT4 isomerization barriers are of similar energies, the predicted branching ratios to these product channels are very sensitive to the *ab initio* barrier heights when the vibrational energy distribution of the dissociating radicals spans these barriers. In our previous study on this system, which did not include all the relevant isomers of the key radical intermediates, our RRKM results predicted that the H+acrolein channel would contribute nearly 40% to the product branching. This expanded study includes both the *cis* and the *trans* conformers of the key intermediates and their associated transition states, and it uses improved CCSD(T) calculations. Even though the barriers only changed by 1–2 kcal/mol, the predicted branching fraction to the H+acrolein channel decreased to 28%, closer to the experimentally measured value of 18%. The revised branching prediction used MULTIWELL to properly account for both isomers and population transfer between them. The increased accuracy of the electronic structure calculations impacted the final results significantly as well. Although we used a large basis set (aug-cc-pVQZ) in the previous work), the extrapolation to the complete one-particle basis set limit performed in this work gave a substantial improvement in the prediction.

Two improvements in the theoretical predictions on this system may shed light on the key dynamics that result in the observed product branching in this study and in the O+allyl bimolecular reaction. Classical trajectory calculations may provide insight into the parts of the PES most often accessed if one begins trajectories at INT1. The best RRKM implementation cannot compensate for missing transition states, and trajectory calculations, even those using a PES calculated at a lower level of electronic structure theory, would reveal any absent stationary points. Classical trajectories would also elucidate any pathways not normally considered in RRKM calculations, such as higher order saddle points or any dynamics which is not well-represented by a statistical assumption. Trajectories my also reveal inadequacies in some of the assumptions made in statistical transition state theories; access to the loose transition state leading to H+acrolein may not be dynamically separated from access to the tight INT1 → INT4 isomerization transition state, as both involve motion of the same H atom. Most strikingly, the predicted branching to the HCCH product channel is less than 2%, but our experiments detect signal at m/e=26, assigned to HCCH, that is the same order of magnitude as the $H_2CO+C_2H_3$ product channel. Finally, quantum calculations may well substantially alter the theoretical predictions because many of the key isomerization transition states in this system involve H-atom motion.

Not all of the discrepancies between our experiments and the theoretical predictions can be solved by more accurate barrier heights and improved dynamical calculations on the ground state C_3H_5O PES. A time-resolved study of the INT1 radical dissociation may help reveal the participation of tunneling through the INT1 → INT4 barrier in the dynamics. The weakest aspect of the experimental method used here is the difficulty of partitioning the measured internal energy of the radicals between vibrational and rotational energies, and the calculated branching ratios are sensitive to this partitioning. We use the approximate relation that the energy imparted to rotation of the radical is $0.4E_T$, where E_T is the energy partitioned to product translation in the C–Cl bond photofission and the multiplicative constant is derived empirically by fitting the velocity distribution of the radicals that dissociated to H+acrolein. A direct measurement of the rotational distribution of the nascent INT1/INT2 radicals before they dissociate is prohibited by the very fast dissociation timescales of these radicals. A full theoretical treatment of the experiment may be preferable, where the calculation begins with the photolytic precursor epichlorohydrin and predicts the excited state C–Cl photofission dynamics and energy partitioning to the C_3H_5O radicals before going on to predict the product branching from the ground and excited state C_3H_5O radicals. However, the currently available *ab initio* methods for excited states of polyatomic molecules are not of sufficient accuracy to offer reliable predictions on such a complex system.

Although this study reports the first absolute photoionization cross section and PIE curve for the HCO radical, our result is uncorrected for the possible contribution of dissociative ionization of the CH_3O coproduct of HCCH to the m/e=29 signal. Our reported branching between these two product channels does allow future investigators to subtract this contribution from the spectrum, once the photoionization spectrum of CH_3O is measured. The photodissociation[53] of CH_3OCl provides a 1:1 source of CH_3O and Cl atoms and offers a route to calibrate the absolute partial ionization cross section of CH_3O radical for this correction. We hope this work will stimulate higher-resolution studies of the photoionization spectrum of HCO using the epichlorohydrin precursor, and a correction for the contribution from CH_3O dissociative ionization.

We end with a simple back-of-the-envelope justification for one aspect of the dynamics revealed in the present experiments. The velocity distributions of the $HCO+C_2H_4$ and $H_2CO+C_2H_3$ products from the dissociation of ground state C_3H_5O radicals detected in this work evidenced a strongly forward-backward peaked angular distribution and a large partitioning to kinetic energy between the products. This high kinetic energy release is not due to repulsive forces after the transition state, but rather to the high rotational energy of the dissociating radicals. Classical conservation of angular momentum $J=I\omega$ dictates that as the C–C bond stretches en route to the bond fission transition state, the classical angular rotational frequency ω of the radical slows as the moment of inertia I increases. At the transition state the attractive force between the separating fragments is zero, and the fragments may recoil in the tangential direction with recoil velocities determined by conservation of angular momentum $J=I\omega=I'\omega'=\mu' v'_{rel} b'$, where b' is the exit impact parameter as the HCO and C_2H_4 (or H_2CO and C_2H_3) fragments separate. This gives a prediction for the energy partitioned to kinetic energy between the products $E'_T=\frac{1}{2}\mu' v'^2_{rel}$ since the classical expression for rotational energy of the nascent reactant radical is $J^2/2I$ (before the C–C bond stretches). Thus, in this simple model, $E'_T(I/\mu'(b')^2)E_{rot}$, and one predicts high kinetic energies between the C–C bond fission products of radicals with high rotational energies.

ACKNOWLEDGMENTS

This work was supported by the Chemical Sciences, Geosciences and Biosciences Division, Office of Basic Energy Sciences, Office of Science, U.S. Department of Energy, under Grant No. DE-FG02-92ER14305 (L.J.B.). Synchrotron beam time and additional funding were provided by the National Synchrotron Radiation Research Center (NSRRC) and Academia Sinica in Taiwan (J.J.-M.L.). We gratefully acknowledge the assistance in data acquisition at the NSRRC beamline provided by Wei-Kan Chen, Wen-Jian Huang, Hsueh-Ying Chen, and Chien-Yu Lien. C. A. Taatjes and T. A. Cool provided us with supplemental data on the high-resolution photoionization spectra of C_2H_4 and C_2H_3 that greatly aided this study.

[1] I. R. Slagle, J. R. Bernhardt, D. Gutman, M. A. Hanning-Lee, and M. J. Pilling, J. Phys. Chem. **94**, 3652 (1990).
[2] H.-C. Kwon, J.-H. Park, H. Lee, H.-K. Kim, Y.-S. Choi, and J.-H. Choi, J. Chem. Phys. **116**, 2675 (2002).
[3] J.-H. Park, H. Lee, H.-C. Kwon, H.-K. Kim, Y.-S. Choi, and J.-H. Choi, J. Chem. Phys. **117**, 2017 (2002).
[4] J.-H. Park, H. Lee, and J.-H. Choi, J. Chem. Phys. **119**, 8966 (2003).
[5] S.-K. Park, L.-K. Kwon, H. Lee, and J.-H. Choi, J. Chem. Phys. **120**, 7976 (2004).
[6] J.-H. Choi, Int. Rev. Phys. Chem. **25**, 613 (2006).
[7] N. Balucani and P. Casavecchia, AIP Conf. Proc. **CP855**, 17 (2006).
[8] (a) F. Leonori, N. Balucani, G. Capozza, E. Segoloni, D. Stranges, and P. Casavecchia, Phys. Chem. Chem. Phys. **9**, 1307 (2007); (b) P. Casavecchia, F. Leonori, N. Balucani, R. Petrucci, G. Capozza, and E. Segoloni, *ibid.* **11**, 46 (2009).
[9] B. L. FitzPatrick, K.-C. Lau, L. J. Butler, S.-H. Lee, and J. J. Lin, J. Chem. Phys. **129**, 084301 (2008).
[10] K. Hoyermann, F. Nacke, J. Nothdurft, M. Olzmann, J. Wehmeyer, and T. Zeuch, Proc. Combust. Inst. **32**, 157 (2009).
[11] B. F. FitzPatrick, Ph.D. thesis, Department of Chemistry, The University of Chicago, 2010.
[12] C. C. Wang, Y. T. Lee, J. J. Lin, J. Shu, Y. Y. Lee, and X. J. Yang, J. Chem. Phys. **117**, 153 (2002).
[13] S.-H. Lee, Y.-Y. Lee, Y. T. Lee, and X. Yang, J. Chem. Phys. **119**, 827 (2003).
[14] J. J. Lin, Y. Chen, Y. Y. Lee, Y. T. Lee, and X. Yang, Chem. Phys. Lett. **361**, 374 (2002).
[15] X. Yang, J. Lin, Y. T. Lee, D. A. Blank, A. G. Suits, and A. M. Wodtke, Rev. Sci. Instrum. **68**, 3317 (1997).
[16] Y. T. Lee, J. D. McDonald, P. R. LeBreton, and D. R. Herschbach, Rev. Sci. Instrum. **40**, 1402 (1969).
[17] N. R. Daly, Rev. Sci. Instrum. **31**, 264 (1960).
[18] A. G. Baboul, L. A. Curtiss, P. C. Redfern, and K. Raghavachari, J. Chem. Phys. **110**, 7650 (1999).
[19] L. A. Curtiss, P. C. Redfern, V. Rassolov, G. Kedziora, and J. A. Pople, J. Chem. Phys. **114**, 9287 (2001).
[20] M. J. Frisch, G. W. Trucks, H. B. Schlegel *et al.*, GAUSSIAN03, Revision C.02, Gaussian, Inc., Pittsburgh, PA, 2003.
[21] J. P. Merrick, D. Moran, and L. Radom, J. Phys. Chem. A **111**, 11683 (2007).

[22] MOLPRO, a package of *ab initio* programs designed by H.-J. Werner and P. J. Knowles, Version 2008.1, R. Lindh, F. R. Manby, M. Schütz *et al.*
[23] G. Knizia and H.-J. Werner, J. Chem. Phys. **128**, 154103 (2008).
[24] T. B. Adler, G. Knizia, and H.-J. Werner, J. Chem. Phys. **127**, 221106 (2007).
[25] K. A. Peterson, T. B. Adler, and H.-J. Werner, J. Chem. Phys. **128**, 084102 (2008).
[26] P. J. Knowles, C. Hampel, and H.-J. Werner, J. Chem. Phys. **99**, 5219 (1993); **112**, 3106(E) (2000).
[27] D. W. Schwenke, J. Chem. Phys. **122**, 014107 (2005).
[28] J. L. Miller, L. R. McCunn, M. J. Krisch, L. J. Butler, and J. Shu, J. Chem. Phys. **121**, 1830 (2004).
[29] P. J. Wilson and D. J. Tozer, Chem. Phys. Lett. **352**, 540 (2002).
[30] J. A. Mueller, B. F. Parsons, and L. J. Butler, J. Chem. Phys. **114**, 4505 (2001).
[31] See supplementary material at http://dx.doi.org/10.1063/1.3475001 for for the tabulated NSRRC bandwidth (provided by Y. Y. Lee) and C_2H_4 photoionization spectrum [provided by Taatjes and co-workers (Ref. 47)] used for our data analysis. It also gives our measured dissociative ionization spectrum for acrolein and a supplemental figure, along with preliminary MCSCF results on the low-lying excited state of the INT 1 radical.
[32] MULTIWELL-2009.3 software, 2009, designed and maintained by J. R. Barker with contributors N. F. Ortiz, J. M. Preses, L. L. Lohr, A. Maranzana, P. J. Stimac, and L. T. Nguyen, University of Michigan, Ann Arbor, MI, http://aoss.engin.umich.edu/multiwell/.
[33] J. R. Barker, Int. J. Chem. Kinet. **33**, 232 (2001).
[34] E. J. Hintsa, X. Zhao, and Y. T. Lee, J. Chem. Phys. **92**, 2280 (1990).
[35] B. Ruscic, personal communication (September 2007). These are unpublished interim results from the Active Thermochemical Tables (ATcT), Version 1.36, and the Core (Argonne) Thermochemical Network, Version 1.064.
[36] P. M. Guyon, W. A. Chupka, and J. Berkowitz, J. Chem. Phys. **64**, 1419 (1976).
[37] NIST webbook, www.webbook.nist.gov.
[38] B. L. FitzPatrick, M. Maienschein-Cline, L. J. Butler, S.-H. Lee, and J. J. Lin, J. Phys. Chem. A **111**, 12417 (2007).
[39] J. V. Michael, M.-C. Su, J. W. Sutherland, L. B. Harding, and A. F. Wagner, Proc. Combust. Inst. **30**, 965 (2005).
[40] S.-H. Jen and I.-C. Chen, J. Chem. Phys. **111**, 8448 (1999).
[41] J. C. Person and P. P. Nicole, J. Chem. Phys. **49**, 5421 (1968).
[42] T. A. Cool, J. Wang, K. Nakajima, C. A. Taatjes, and A. Mcllroy, Int. J. Mass. Spectrom. **247**, 18 (2005).
[43] F. A. Grimm, T. A. Whitley, P. R. Keller, and J. W. Taylor, Chem. Phys. **154**, 303 (1991).
[44] D. M. P. Holland, D. A. Shaw, M. A. Hayes, L. G. Shpinkova, E. E. Rennie, L. Karlsson, P. Baltzer, and B. Wannberg, Chem. Phys. **219**, 91 (1997).
[45] J. M. Dyke, N. B. H. Jonathan, A. Morris, and M. J. Winter, Mol. Phys. **39**, 629 (1980).
[46] J. Wang, L.-X. Wei, R. Yang, C.-Q. Huang, X.-B. Shan, L.-S. Sheng, Y.-W. Zhang, F. Qi, C.-d. Yao, Q. Li, and Q. Ji, Chem. Res. Chin. Univ. **22**, 375 (2006).
[47] C. A. Taatjes, private communication (2008).
[48] J. C. Robinson, N. E. Sveum, and D. I. M. Neumark, J. Chem. Phys. **119**, 5311 (2003).
[49] D. S. Peterka, private communication (2002).
[50] M. W. Crofton, M. J. Jagod, B. D. Rehfuss, and T. Oka, J. Chem. Phys. **91**, 5139 (1989).
[51] C. M. Gabrys, D. Uy, M. F. Jagod, T. Oka, and T. Amano, J. Am. Chem. Soc. **90**, 15611 (1995).
[52] J. N. Harvey and M. Aschi, Phys. Chem. Chem. Phys. **1**, 5555 (1999).
[53] M. J. Krisch, L. R. McCunn, K. Takematsu, L. J. Butler, F. R. Blase, and J. Shu, J. Phys. Chem. A **108**, 1650 (2004).
[54] P. Casavecchia, Rep. Prog. Phys. **63**, 355 (2000).